FEASIBILITY INVESTIGATION OF A LOW-TEMPERATURE, VARIABLE INFRARED SOURCE

Horizon Definition Study

GPO PRICE $

CFSTI PRICE(S) $

Hard copy (HC)

Microfiche (MF)

ff 653 July 65

Distribution of this report is provided in the interest of information exchange. Responsibility for the contents resides in the author or organization that prepared it. Funding limitations precluded complete testing of the variable infrared source, and the results should be viewed as preliminary.

March 1968

Prepared under Contract NAS 1—6010 by

HONEYWELL INC.

Systems & Research Division

Minneapolis, Minn.

for

NATIONAL AERONAUTICS AND SPACE ADMINISTRATION

FEASIBILITY INVESTIGATION OF A
LOW-TEMPERATURE, VARIABLE INFRARED SOURCE

By Joseph S. Titus
Roger N. Schmidt

HORIZON DEFINITION STUDY

March 1968

CONTENTS

ILLUSTRATIONS

FEASIBILITY INVESTIGATION OF A
LOW-TEMPERATURE, VARIABLE INFRARED SOURCE

By Joseph S. Titus
Roger N. Schmidt

SUMMARY

A requirement for a variable-temperature, highly accurate infrared source
has been identified for the Horizon Definition Study. A survey of the state of
the art indicated that no system was available to satisfy this requirement.
An analysis was performed, subassembly tests conducted, and a system
designed and fabricated to verify the analysis. Preliminary test results
indicate that, although problem areas still exist in the implementation of this
device, the requirements can be met.

INTRODUCTION

Calibration, defined as the measurement of the voltage-radiance transfer characteristic of an instrument, is one of the limiting factors in using infrared data for definition of the earth's horizon. The position described as the horizon by an instrument relying upon radiance for its measurement has an error which is directly attributable to the error in calibrating the instrument.

It has been shown (references 1 and 2) that the optimum wavelength region for horizon definition is the 15μ CO_2 absorption band. Theoretical analysis and corroborative experimental data have given the range of radiance in this wavelength interval as being equivalent to that of a blackbody in the same wavelength interval with a temperature between 100 and 250°K. The error requirements on the calibration source to meet the requirements of horizon definition are such as to require experimental verification of the temperature measurement capability and of the radiation characteristics of the system. There are no calibration devices presently available with both the operating regime and the required error performance.

There are three general techniques in use in infrared calibration:

a) The point-source technique, where the source subtends an angle less than the resolution element of the system being calibrated. Variation in source output is obtained with a variable aperture plate. Use of this technique in calibrating an instrument which is required to measure an extended source (i.e., a source whose angular subtense is larger than the resolution of the instrument) requires an accurate knowledge of the elemental field of view of the instrument.

b) The extended-source technique, where an extended source, without an optical system, is used. This technique has the disadvantage of not filling the optical aperture of the system and hence uses only a portion of the optics. This disadvantage can be overcome by making the source sufficiently large that the source itself fills the aperture. For large instruments, this has the obvious disadvantage of requiring low thermal gradients over large areas.

2

c) The extended source at infinity. Here a relatively small source is placed at the focus of a collimating optical system. The collimated beam is of sufficient diameter to fill the optical aperture, and the source is imaged as an extended source.

There are two ways of obtaining a variable extended source, either by varying the temperature of the source, or by using a constant-temperature source and interjecting an attenuator in the optical path. The latter approach requires development of two devices, the source itself and the attenuator. Because of this and because National Bureau of Standards (NBS) is developing a constant-temperature source, the investigation described below is limited to a variable-temperature source.

A variable-temperature source has been designed and a feasibility demonstration prototype constructed and tested for operation in the temperature range discussed above. The source is constructed of copper, relying on high thermal conductance to minimize thermal gradients. Testing has included thermometry, conductance, and radiation mapping of the source. An analysis of gradients and experimental measurement indicates that, with adequate isolation, the gradient requirements can be met. The radiative measurements have corroborated the analysis to the precision of the measurements.

REQUIREMENTS AND DESIGN SUMMARY

During the Phase A, Part II conceptual design study for the Horizon Definition Study (HDS), infrared calibration was identified as a critical element in the demonstration of HDS measurement system feasibility. A survey of existing artificial sources indicated that no long-wavelength standard with suitable characteristics was available off-the-shelf. The basic requirement is energy content in the 14 to 16μ wavelength interval between 0.01 and 7.0 W/m^2-sr. This corresponds to blackbody temperatures in the range 100 to 270°K. As can be seen from Table 1, there are no commercial devices available with temperatures in this range. A feasibility investigation of calibration systems resulted in selection of the following three approaches for more detailed study:

- A variable-temperature source
- A constant-temperature system with a diffuser-plate attenuator
- A fixed-radiance source using the slush point of mercury.

TABLE 1. - SURVEY OF OFF-THE-SHELF ARTIFICIAL SOURCES

Mfr. model no.	Type of radiation source	Temperature Range, °C	Temperature Accuracy, °C	Field of view, deg	Aperture diameter	Emissivity	Warm-up time, minutes, temperature, °C	Max. input power, W	Temperature measuring element	Radiance inaccuracy, %	Life
Barnes 11-101	14° conical cavity	0-230	±1	20	0.625 in. 16.9 mm	.99 ±1%	30 230	100	Pt		Long
Perkin-Elmer PE 521-4 (source) PE 521-5 (controller)	15° conical cavity	50-600	±1	20	0.50 in. 12.7 mm		20 600	160	Pt		Long
	Blackened silver cone										
ITT	Blackened conical cavity	40-300	±1		0.375 in. 9.5 mm				Tc		Long
NBS	Tin Zinc	500°K 700°K	±.017 ±.017		3/8 in. 3/8 in.	.9997 .9997		500 500			Primary standard Primary standard
NBS	Flat plate	Basically an emissivity standard									
IRI Ind. IRI 412 (source) IRI 106 (controller)	Blackened conical cavity	50-900	±1	90	4.5 x 4.5 in. 114.3 x 114.3 mm	.90-.97	60	800	Pt	2.0	Long
NBS	Carbon	2000									50 hr (1%)
NBS[a]	Tungsten filament quartz envelope	2700						.75 A ~100 W		0.6	50 hr (1%)

[a] Radiance is 570 μ W/cm² at 1 m.

4

The variable-temperature source has spectral content dependent upon temperature and provides a partial calibration of the spectral characteristics of the device being calibrated. The constant-temperature source has constant spectral content and serves as a check on the calculations of spectral output of the variable-temperature source. The fixed-radiance source provides a double check against the two variable sources, relying neither upon temperature measurement and control nor upon mechanical attenuators for its control of radiance output. By itself, development of this device would not demonstrate feasibility, since this is a single-point calibration only. Of these three approaches, the variable-temperature source presents the simplest design and test problem.

A preliminary investigation indicated that the state of the art in thermometry and design of high-emissivity cavities was sufficiently far advanced to yield results in the accuracy range required. The constant-temperature system, using the melting point of tin (500°K) as a temperature reference, is under development by NBS. Development of the attenuator required for the constant-temperature source without a developed source is not practical in terms of results sufficiently early to demonstrate HDS feasibility. Accordingly, development of the variable-temperature source was undertaken.

The power per unit area radiated into a hemisphere from a graybody of emittance ε at absolute temperature $T(°K)$ is given by the Stefan-Boltzmann law:

$$R = \varepsilon (\lambda, T) \sigma T^4 \; W/m^2$$

where

$$\sigma = \text{Stefan-Boltzmann constant}$$
$$= 5.6687 \times 10^{-8} \; W/m^2\text{-}°K^4$$
$$\varepsilon (\lambda, T) = \text{emittance as a function of wavelength and temperature}$$

The spectral radiance (in $W/m^2\text{-}\mu$) for a blackbody is given by the Planck radiation formula:

$$R_{bb} \; d\lambda = \frac{2\pi c^2 h}{\lambda^5 [\exp (hc/\lambda^2 T)-1]} \; d\lambda$$

where

$$h = \text{Planck's constant}$$
$$= 6.6252 \times 10^{-34} \; J\text{-sec}$$
$$\lambda = \text{wavelength}$$
$$c = \text{speed of light}$$

For the HDS system, the spectral interval 14.00 to 16.28μ with radiance levels between 0.01 and 7.0 W/m^2-sr is specified. Figure 1 shows the radiance for a blackbody in this spectral interval over the operating temperature range.

REQUIREMENTS

The calibration feasibility demonstration system design was conditioned upon the following general requirements:

- The system is required to operate in conjunction with an f/5 collimator in vacuum.

- The system must operate over the temperature range of 100 to 250°K.

- Set-up and settling times shall be such that at least eight readings can be taken in one working day to provide a calibration within reasonable cost and schedule constraints.

- The system must operate with a scale (percentage) error of less than one percent in radiance and with a bias (zero offset) error of less than 0.01 W/m^2-sr, and the system shall be designed to meaure these errors. These requirements are derived from the measurement system requirements for the HDS radiometer and represent an order of magnitude improvement over present state of the art.

Error Allocations

An error analysis of a conceptual calibration system was performed (ref. 3). This system (Figure 2) consists of a variable temperature source with low-speed chopper, a collimator to provide an image at infinity, a shrouded chamber, and a shrouded radiometer.

Scale error sources were identified as:
- Collimator reflectance
- Source emittance
- Temperature

Bias error sources were identified as:
- Chopper emission
- Collimator emission
- Radiometer emission reflected off chopper blade
- Chamber radiation reflected by chopper
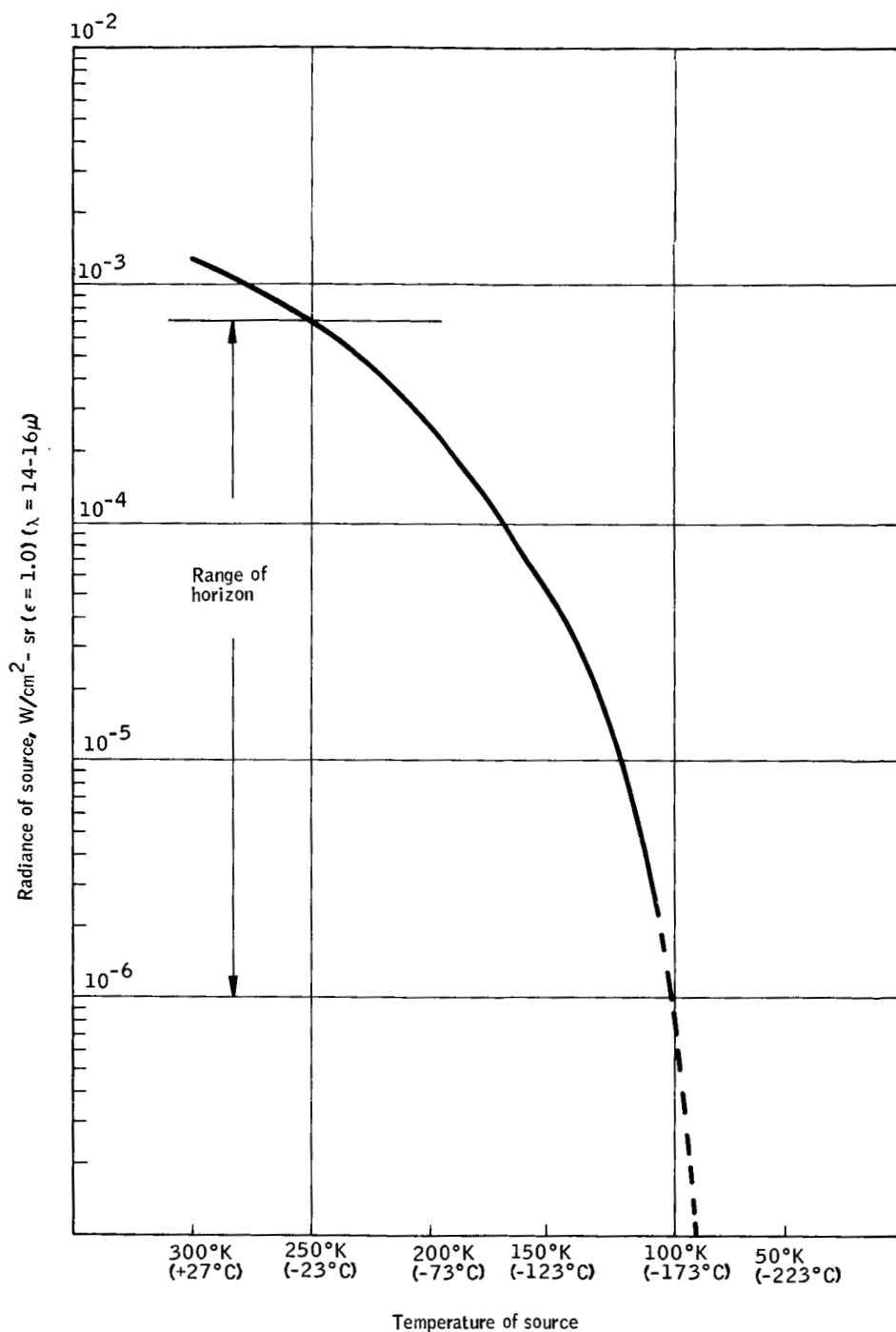
Figure 1. Radiance of Blackbodies, λ = 14 to 16.28μ, as a Function of Temperature
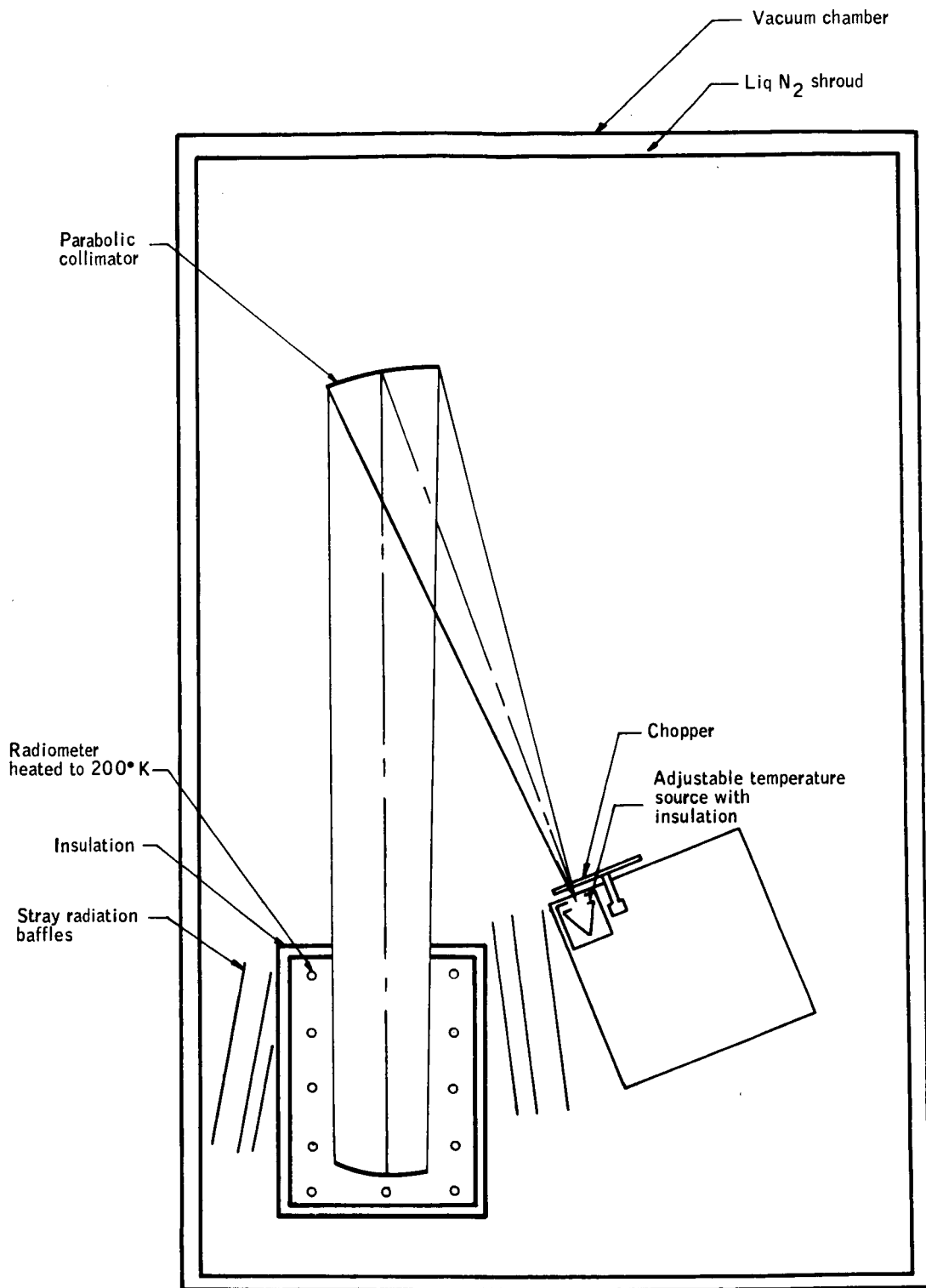
Figure 2. Apparatus for Primary Calibration Using the Adjustable
Temperature Source

Scale errors. -- Errors affecting the scale, i. e., errors resulting in constant multiplicative effect, have been identified as:

a) Error in collimator reflectance - The maximum error was estimated as 0.187 percent.

b) Source emittance - The error in calculated radiance is directly proportional to the error in emittance. The subsequent section, Cavity Design, treats the calculation of emittance in detail. An initial error allocation of 0.1 percent (emittance of at least 0.999) was made.

c) Temperature - Figure 3 is used as the basis for definition of the temperature error requirements. This figure gives the percent error in radiance at 15 microns as a function of temperature error and absolute temperature. Included on this figure is the percent error in radiance due to detector noise, where the noise is that specified for the HDS radiometer, 0.003 W/m^2-sr. Also given on the right-hand ordinate is the emittance corresponding to percent error. Emittance and radiance error are related simply as complements, i. e., emittance error is separable from temperature error. As discussed above, emittance error is allocated at 0.1 percent.

Initial estimates of practically obtainable temperature errors of 0.05°C at liquid-nitrogen temperatures and 0.01°C at room temperature were made, yielding errors of 0.6 percent at liquid-nitrogen temperatures and 0.01 percent at room temperature from Figure 3. These allocations are extremely conservative. After deducting collimator reflectance (0.187 percent) and emittance (0.1 percent), an error of 0.7 percent is left as a remainder from the required bias error. There is no reason to make the radiance bias error smaller than the HDS detector noise. If the requirement is restated as 1.0 percent error or HDS detector noise, whichever is greater, this requirement is easily achieved with a temperature error of 0.1°C; i. e., the curve of 0.1°C lies below 0.7 percent error until past the intersection with the detector noise error curve. To permit a margin for unidentified error sources, the temperature measurement requirement is taken as 0.05°C.

Bias errors. --

● Chopper emission - A low emissivity chopper operating at approximately liquid-nitrogen temperatures gives
1.6 x 10^{-8} W/cm^2-sr.

● Collimator emission = 1.66 x 10^{-8} W/cm^2-sr.

● Radiometer emission reflected off chopper blade - Only the diffuse component is reflected. Estimated 0.1 percent diffuse reflectance in direction of radiometer yields
2.6 x 10^{-9} W/cm^2-sr.

Comparison of radiance errors (monochromatic at 15μ)
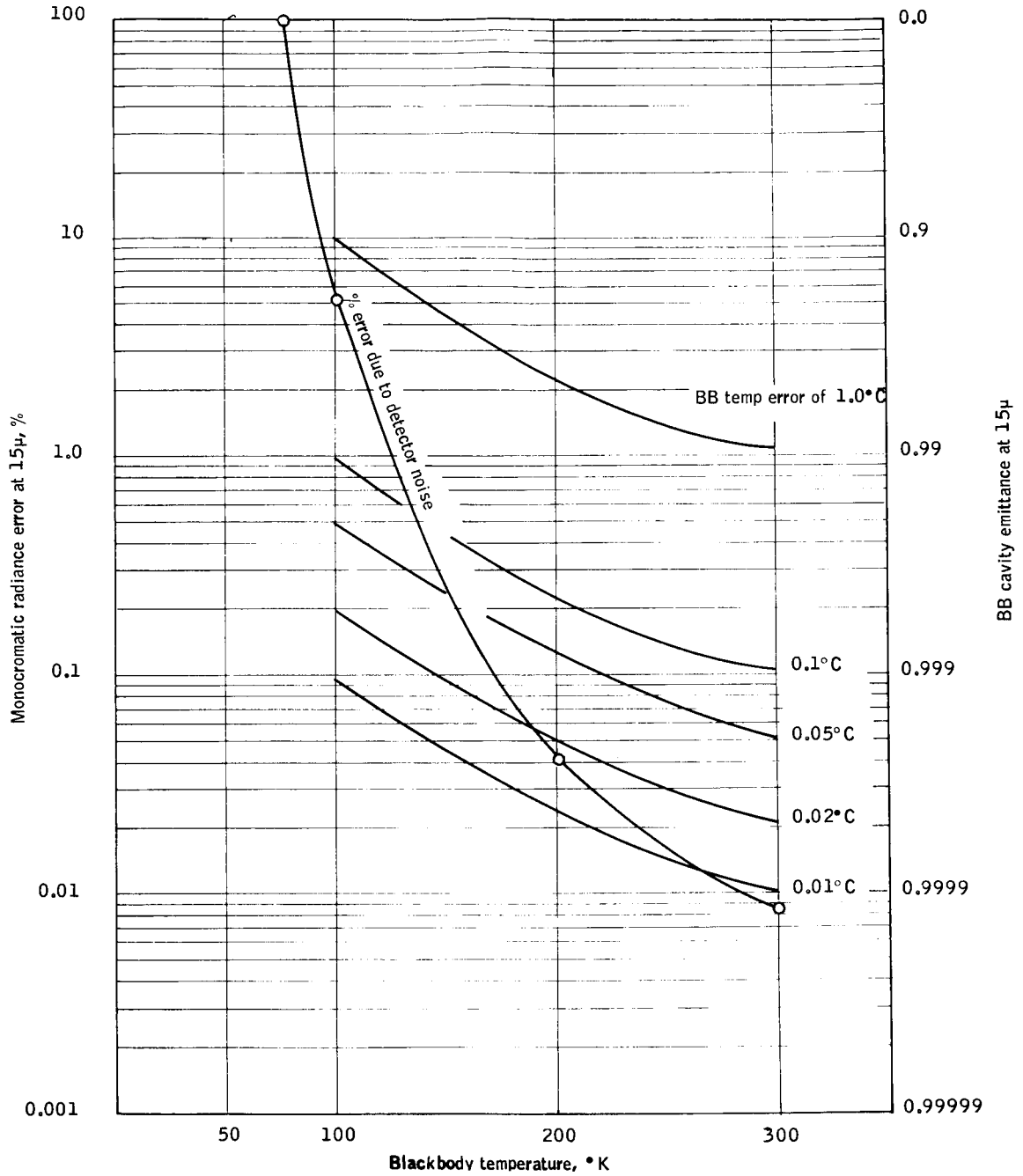
Figure 3. Radiance Error Due to Temperature Error

- Chamber radiation reflected by chopper = 8.3×10^{-7} W/cm^2-sr.

- Total bias errors (linear sum) = 8.75×10^{-7} W/cm^2-sr.

Source Gradient Errors

The errors listed above are identified with the temperature and emissivity of the local region on the source aperture subtended by the radiometer field of view. Clearly, the gradient structure of the source must be such that at no point in the aperture is the radiance incorrectly labeled by more than the allowances given above. Standard practice in dealing with emissive surfaces relegates errors of this type to an effective emissivity, holding the average temperature as an invariant parameter. Using this approach, the requirement is that no region on the aperture of the order subtended by the HDS radiometer have average emissivity less than 0.999, which, referencing Figure 3, gives 0.1 percent error.

The smaller dimension of the field stop in the HDS radiometer (reference 3) subtends 0.04 cm with an f/5 collimator. The requirement on gradient errors then is that the emittance gradient be less than 0.002 per 0.04 cm or 0.05 per cm, and this refers only to local gradients, i. e., with this slope the length of the gradient cannot exceed 0.04 cm.

A conceptual calibration system design was described in Phase A, Part II and is shown in Figure 4. To minimize gradients, a copper block with a cavity machined into the block was proposed. To obtain the requisite temperature accuracy, a laboratory standard platinum resistance thermometer was immersed in a silicone oil well in the block. Temperature control was by direct heating of the block with a nichrome heater controlled by a time-proportional heater controller, operating from an auxiliary thermometer.

This report covers the detailed design exercise which culminated in the design shown in Figure 5. The copper block - standard platinum thermometer initially recommended has been retained. Two capsule standard thermometers 1.5 inches long were used in place of the single 12-inch laboratory standard. The capsule thermometers permit a direct measure of the thermal gradient structure of the block and provide a check against calibration shifts.

Silicon oil was found to be unsuitable for thermal coupling of the thermometer because of a chemical change to an insulator at liquid-nitrogen temperatures, and a beryllium-copper spring thermometer carrier assembly was substituted.

The cavity has been specially designed for use with an f/5 collimator, i. e., it has a 10° emittance cone.

For high emittance with a direct view of the tip, a very small radius must be obtained, since the tip acts as a spherical mirror for on-axis rays. The design utilized calls for an off-axis cone to avoid a direct view of the cone tip. The cavity is coated with a high-emittance, specular epoxy.
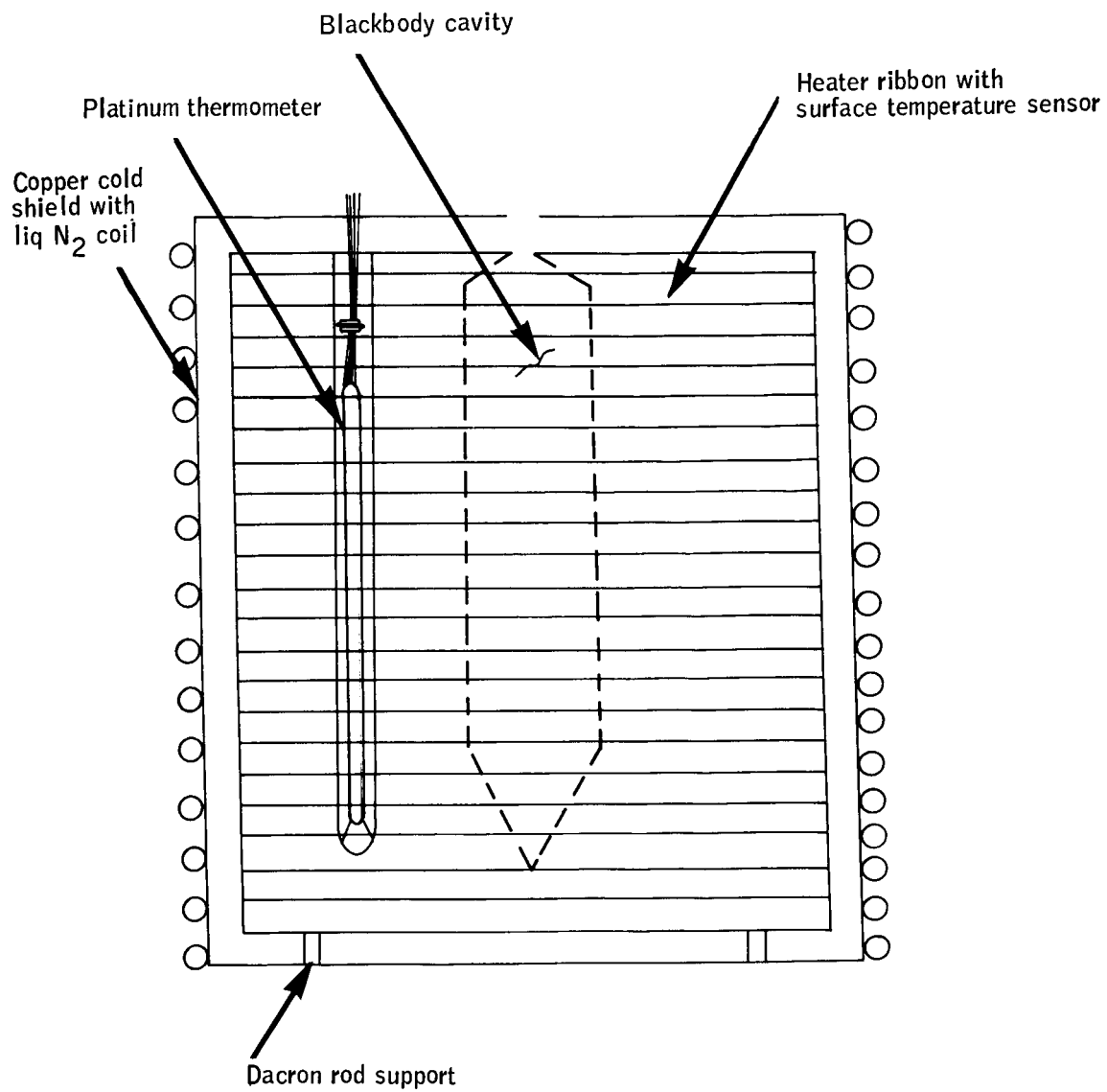
Figure 4. Initial Conceptual Design

12

Dewar

Guard
heater

Sin
rad

Platinum
thermometers

Screwjack
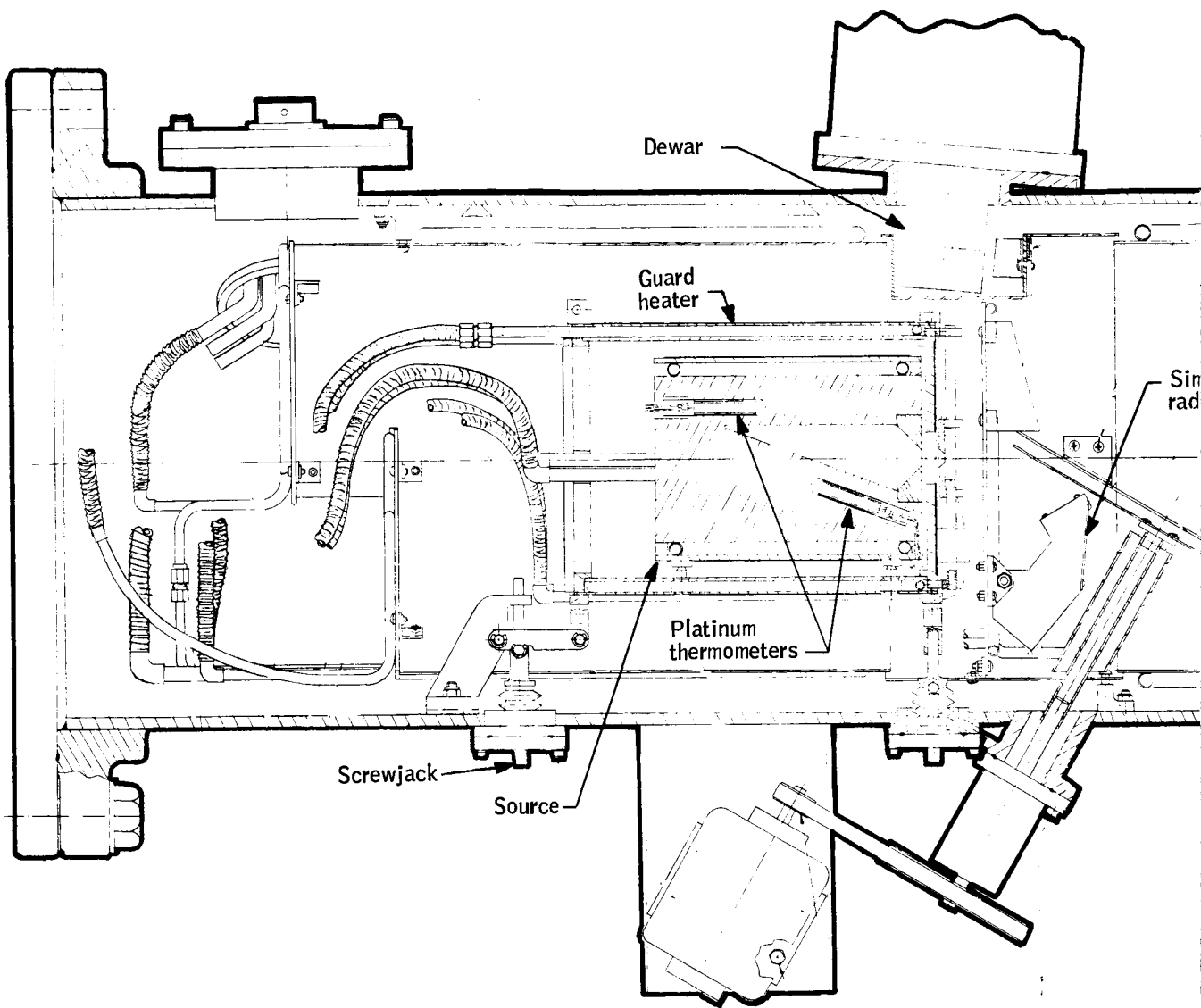
Source

Figure 5. Final Design of Va
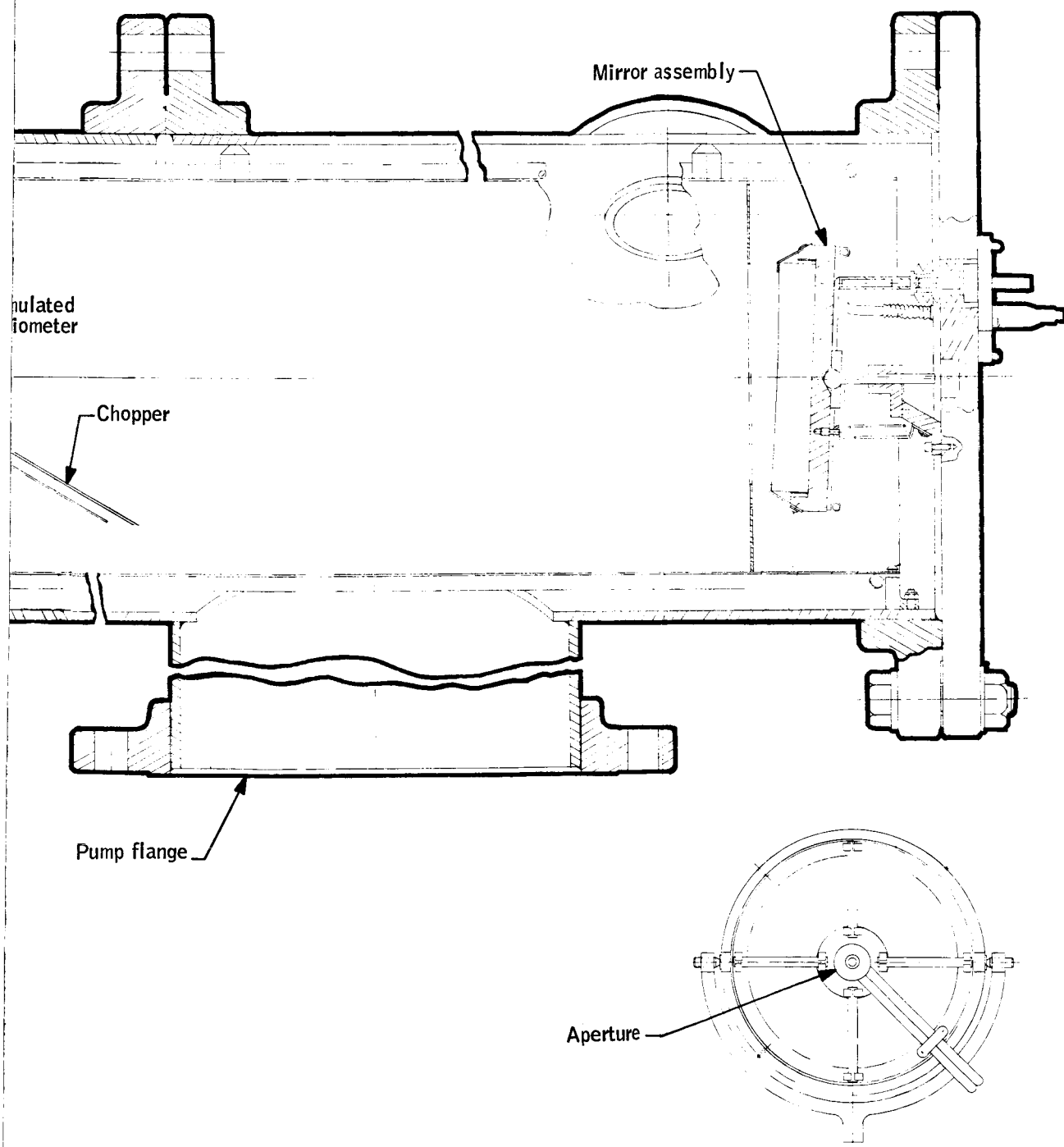
Mirror assembly

ulated
iometer

Chopper

Pump flange

Aperture

riable - Temperature Source

The heater system uses a spray-on heater and liquid-nitrogen coils. Block temperature is adjusted with a heater applied to a cylinder pressed onto the block. Direct heating and cooling of the block is used only for changing the block temperature and not for temperature control. During a measurement, the block is maintained at constant temperature by a guard heater, which is essentially an active insulator. The guard heater is a cylindrical assembly coupled to the block radiatively and controlled to the block temperature. Thus, the block "sees" a temperature gradient which is the difference in temperature between the block and the guard, approximately 0.1°C. With this system, block temperature drift of the order of millidegrees per minute can be obtained.

TECHNICAL DISCUSSION

The technical areas investigated may be categorized as:

- Thermometry
- Radiometry
- Cavity design
- Supporting systems

Thermometry is defined as the problem of reading the temperature of a radiating surface with devices which cannot be perfectly coupled to the surface. Errors will be generated by the measurement process itself and by the devices not being in perfect calibration with the temperature scale used in the physical laws defining radiance.

Radiometry is the measurement of the spatial and angular characteristics of the radiation field.

Cavity design is essentially the analysis of radiative properties of geometrical shapes and the selection of a cavity and coating to meet the emittance requirements established above.

The supporting systems are the vacuum chamber, mechanisms for obtaining motion of the source to permit radiometric measurements, the thermal control system simulated radiometer, and liquid-nitrogen shrouds.

THERMOMETRY

As discussed above, the errors in radiance allocated to thermometry yield a temperature measurement error of approximately 0.05°K. These errors must be defined relative to the thermodynamic scale to be meaningful for use in the Stefan-Boltzmann equation. The standards for thermometry are defined in terms of a series of baths, and the scale so defined is known as the International Practical Temperature Scale (references 4 and 5). The only point on these two scales which is in exact correspondence is the triple point of water (0.01°C). At 0°C the two scales correspond to within 0.001°C.

The NBS gives data (Figures 6 and 7) which indicates that the maximum error is no greater than one part in 10^4 at the low end of the scale, or 0.010°. Rosemount Engineering, the thermometer supplier, gives data which indicates a maximum calibration error of 0.010° (Figure 8). The basic, unremovable temperature measurement error is then approximately 0.020° worst-case. The other error sources identifiable in the thermometry system are the thermometer coupling error, gradients between the thermometers, and the measurement error itself. With standards laboratory equipment (G-2 Mueller Bridge) measurement, accuracy of approximately 1 millidegree is obtainable, and this error does not enter into the problem significantly. An allocation of 0.01° to the error due to coupling and the error due to gradient, respectively, was made.

The thermometry problem for the system is that of measuring the average temperature of an emitting surface with a thermometer which by its construction is not a surface-measuring device. A series of analyses and experiments were conducted to demonstrate that the thermometer is indeed measuring the surface temperature of the cavity.

A thermal equivalent circuit of the thermometer system is shown in Figure 9. Since there is heat flow in the system in thermal equilibrium, stable temperature gradients will exist in the system. The major sources of gradient-forcing heat flow are radiation from the cavity and conductive flow along the thermometer leads. An analysis was made of the possible gradients across the coating. Extreme ranges for the conductivity of the coating of 1 Btu/hr/ft/°F and 0.1 Btu/hr/ft/°F were assumed. In the worst-case for radiance (300°K source radiating to zero), the power leaving the aperture is 0.127 Btu/hr. This power is assumed to be uniformly distributed over the aperture. A paint thickness of 1 mil (0.001 inch) was assumed. Calculated gradients were 0.00005°C for the lower conductivity of 0.1 Btu/hr/ft/°F. The worst of these values is 1.5 orders of magnitude below the error requirements. Therefore, it is assumed that gradients across the cavity coating are negligible.

The copper block was analyzed to determine if the thermal conductivity of the block was sufficiently high that gradients of the order of 0.01°C were not obtained. An extreme case was analyzed. Heat loss was assumed to have all occurred at one end of the block and to have been generated at the other end. For a total load of 0.0454 Btu/hr loss through the support structure and an aperture radiative flux of 0.127 Btu/hr, the calculated gradient was 0.003°C. These calculations were verified experimentally (see Appendix A).

16
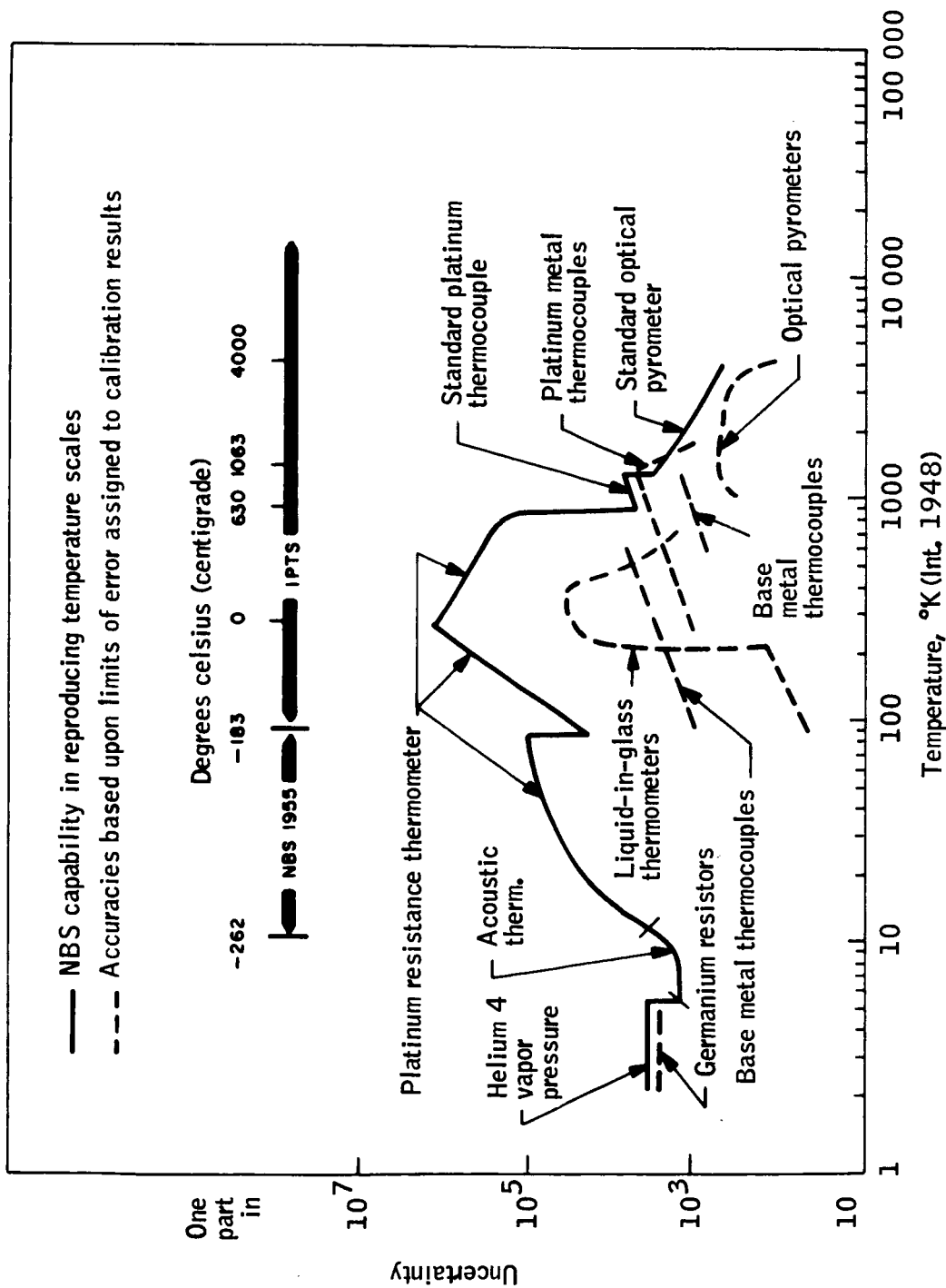
Figure 6. Calibration of Temperature-Measuring Instruments (From NBS Technical Note 262, p. 14)

17
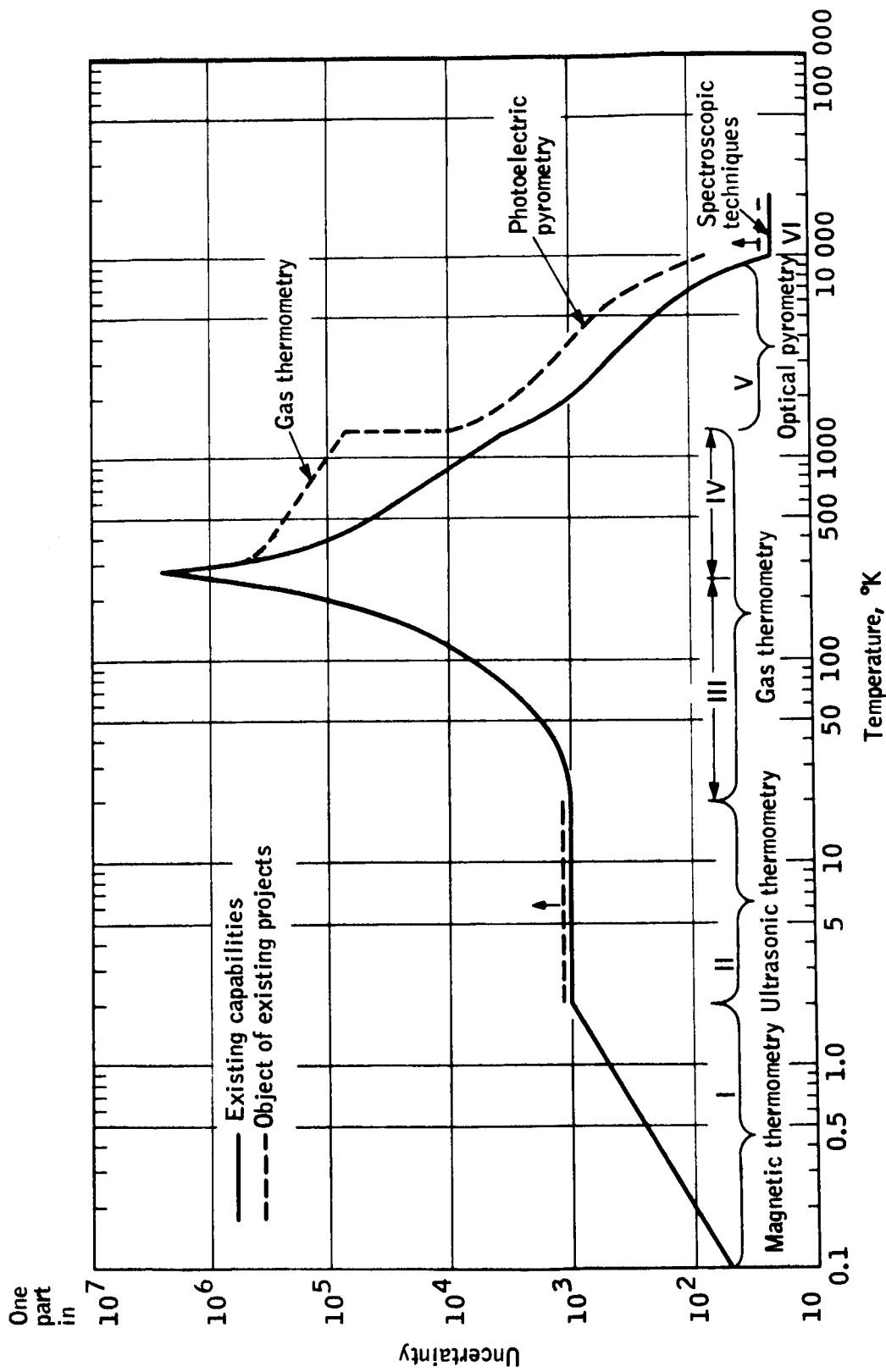
Figure 7. Accuracy of Realization of the Thermodynamic Temperature Scale (From NBS Technical Note 262, p. 12)

18
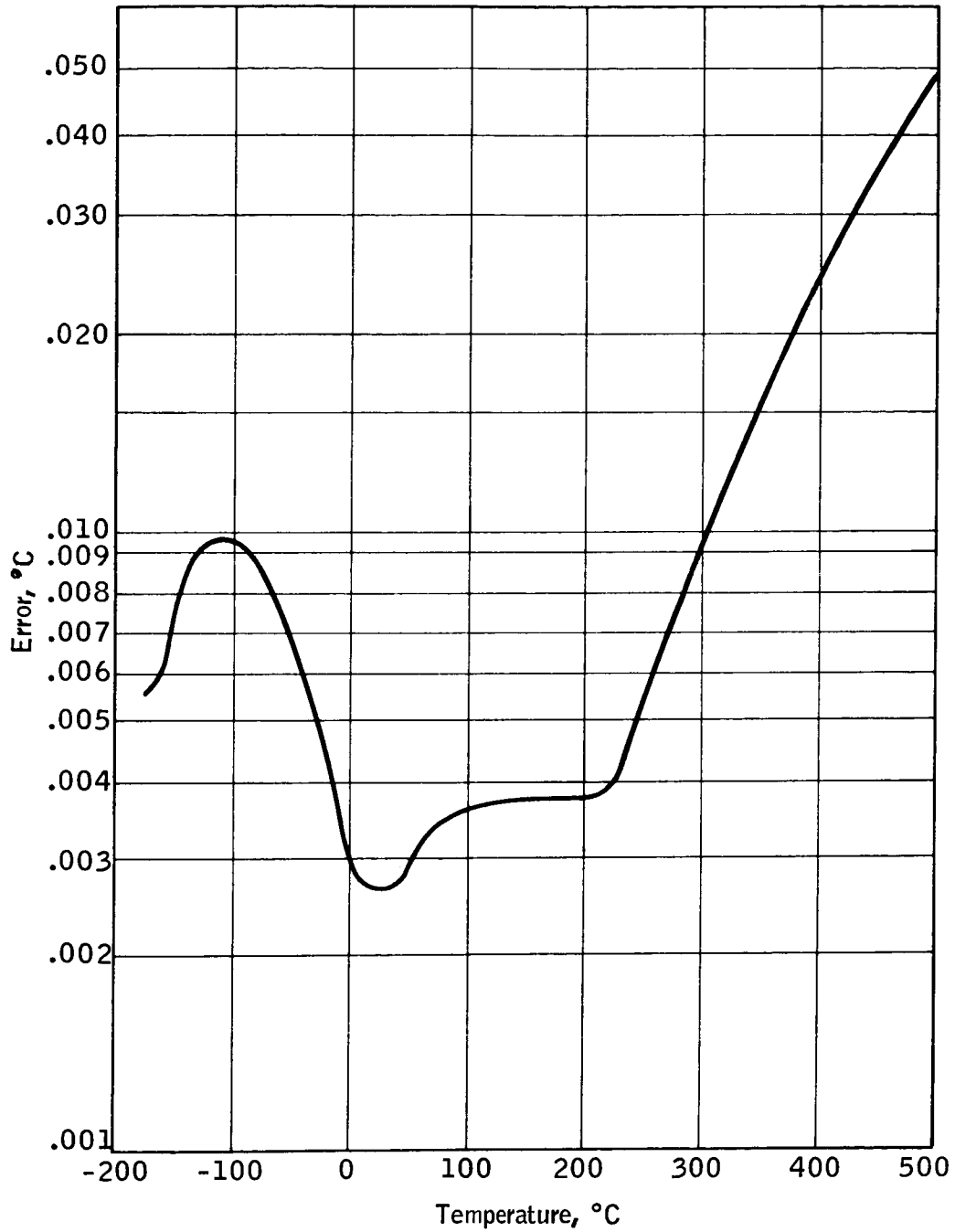
Figure 8. Calibration Accuracy of Platinum Thermometer (From Rosemount
Engineering Company, Temperature Standard 162D)
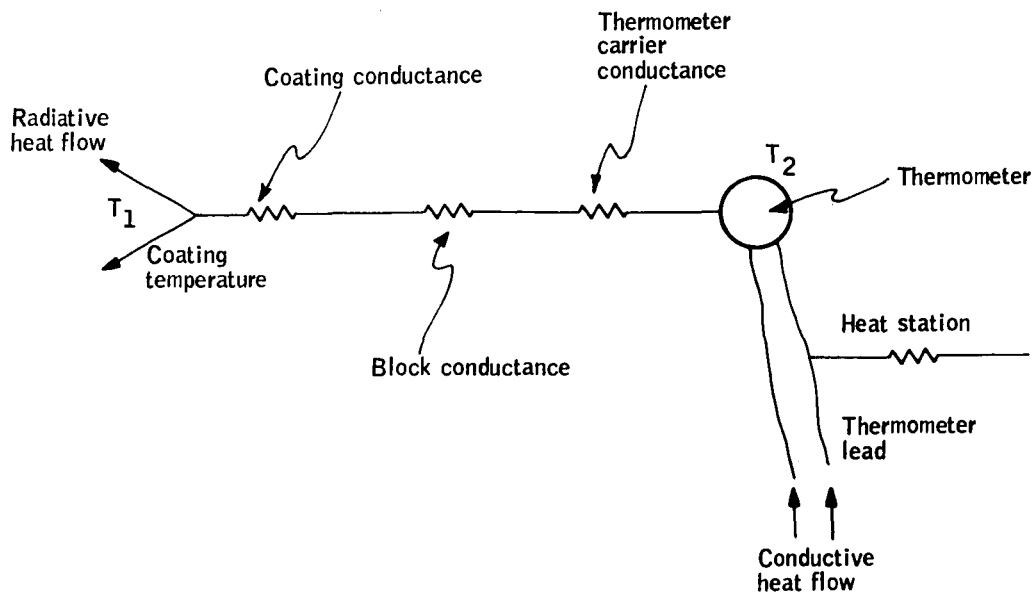
Figure 9. Thermal Equivalent Circuit of Thermometer System

The thermometer carrier conductance was established empirically. (This topic is discussed in a later section of this report.) Numerical results obtained agree closely with other reported experimental data. A carrier conductance of approximately 0.054 W/°C was obtained, which imposes a requirement for stationing the wires with a ratio of conductance (heat station to thermometer carrier) of 36:1. The primary source of heat for the thermometer is conduction through the leads. Worst-case is clearly when the block is near liquid-nitrogen temperatures. The leads are heat-stationed on the block itself and on the guard heater. The heat-stationing in this case uses five wraps of the block and five wraps of the guard heater, both tied with Beta (fiberglass) cord.

The thermometers installed in the system are Rosemount Engineering Corporation (REC) Platinum Resistance Standard Model 162 Dx, Serial Nos. 631 and 633. The thermometers were calibrated at REC according to the following schedule:

● Liquid nitrogen

● Liquid oxygen

● Water triple point

A check calibration in an ice bath was made at Honeywell. The calibrations agreed to within 0.001°C.

The thermometers are installed in a split carrier with beryllium-copper leaf-spring thermal contact. The thermometer is a tight slip-fit in the split-ring, which runs the length of the thermometer. Two leaf-springs run the length of the split-ring and are compressed for insertion in a 3/8-inch-diameter hole. This technique was required in lieu of mechanical clamping because of the high compressive loads encountered over the 200°C operating range. The thermometers are positioned at the front and below and at the rear and above the machined cavity to define the gradiant structure of the system.

These thermometers are of a four-lead configuration designed for operation with a Mueller bridge. The lead configuration allows removal of the lead resistance from the measurement.

RADIOMETRY

Because of the difficulty of measuring the absolute emittance of the system directly, the relative goniometric characteristics were measured with a radiometer, and the absolute emittance was established by calculation.

The radiometer design was conditioned primarily upon the requirement that the design be as simple as possible (i. e., minimum number of emitting surfaces) and that the radiometer be capable of sensing radiance differences of 0.01 W/m^2-sr. An f/5 spherical mirror was used as the single optical element in the system.

The optical system was designed such that both the cavity defining aperture and the detector are at a distance equal to the mirror radius of curvature away from the mirror and equidistant off axis on opposite sides of the optical axis so that the cavity aperture is imaged at the detector. At this point spherical aberration is negligible, and the system is primarily astigmatic. A ray trace of this system was obtained and is shown in Figure 10. The requirement on blur circle is that it be approximately one-tenth of the defining aperture to permit mapping of the aperture. The aperture is 0.5 cm and the blur circle should be of the order of 0.05 cm (0.5 mm). From Figure 10 it can be seen that this requirement is easily met by this system. The system operates at unity magnification, and the detector size should then also be of the order of 0.5 mm. Focus and alignment are obtained with three micrometer screws feeding through stainless bellows, acting against spring-loaded fiberglass fingers which form a three-point mount for the gold coated, quartz mirror. The mount is cooled with liquid nitrogen.

The detector is copper-doped germanium, 0.5 mm in diameter, cold-shielded to a 10° field of view. The detector, cold shield, and narrow-band filter are mounted in an SBRC 9145-1 liquid-helium Dewar, with a three-inch side-looking snout. The filter is a standard OCLI filter, giving response from 14 to

21
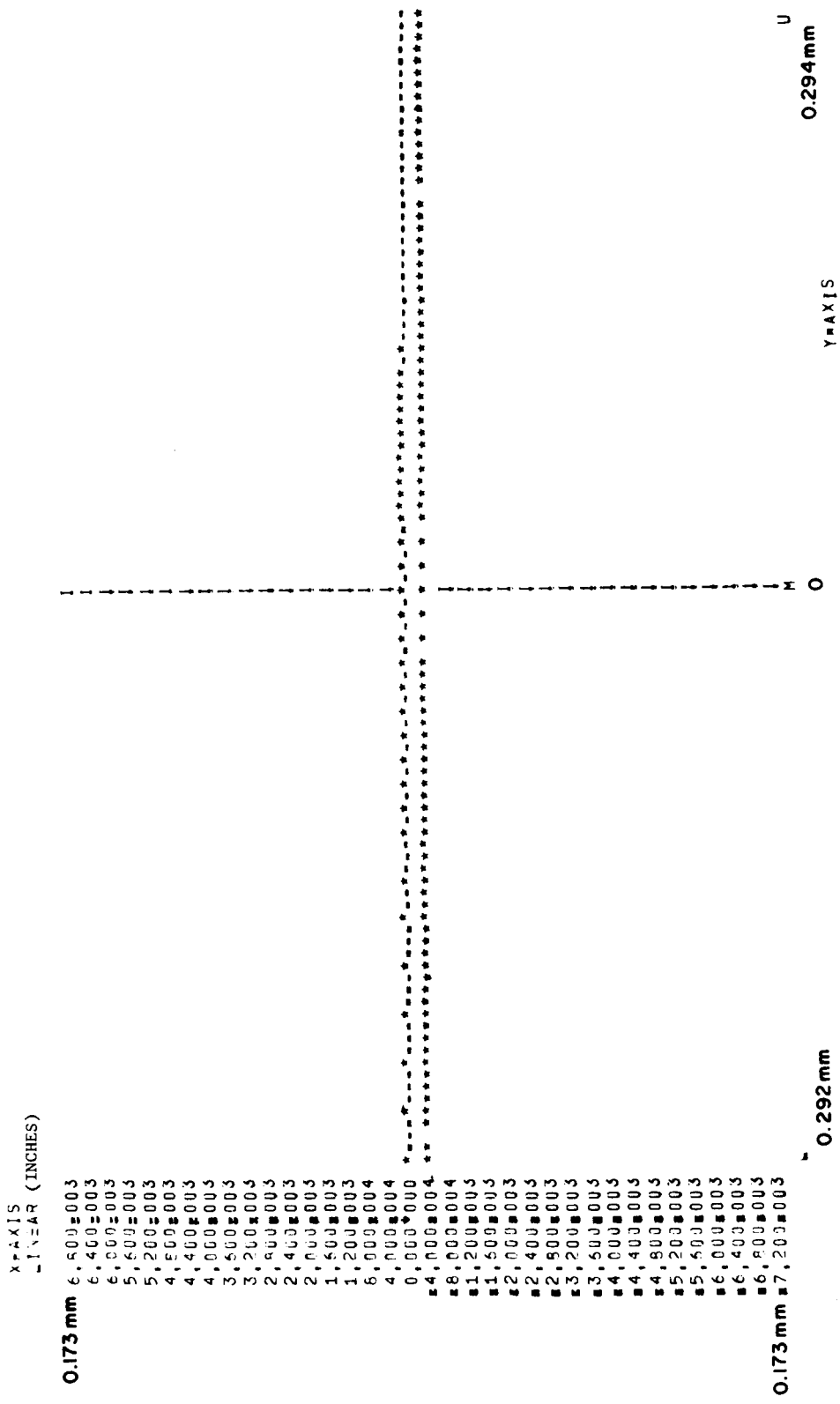
Figure 10.   Spot Diagram - f/5 6-inch Spherical Reflector 3-degree Off-Axis Object at Radius of Curvature

16μ at liquid-helium temperature. A wide-band blocking filter (11 to 18μ transmission) held at liquid-nitrogen temperatures is inserted in the field. A spectral scan of the 14 to 16μ filter and detector and measured detector performance are given in Appendix B. A spectral scan of the filter only is shown in Figure 11.

Doped germanium exhibits 1/f noise to approximately 100 Hz; hence a chopper system is required to obtain high detectivity. The size of the aperture dictated the use of a rotating chopper. To avoid operation of a motor in a vacuum, a bellows drive was used with external drive from an 1800-rpm synchronous motor. The bellows drive is limited to 500 rpm, and with chopper dimensions to fit the chamber, a maximum chopping rate of 100 Hz is obtained. A margin was obtained by driving the system at 480 rpm, yielding 96 chops per second.

The chopper is a toothed wheel, constructed of 0.04-inch aluminum. Blade diameter is 8.25 inches and tooth depth 1.25 inches. The chopper is driven through a four-inch hollow fiberglass shaft to eliminate heat conduction to the blade. The blade is shrouded to eliminate possible multiple reflections. The teeth are polished aluminum on both sides. The chopper below the teeth is coated with 3M Black Velvet for radiative cooling. This provides minimum interaction of the blade with the cavity and, by inclining the blade, permits the use of an auxiliary absorbing cavity to eliminate backscatter from the radiometer being calibrated. The chopper blade is radiatively cooled and is coated both sides with 3M Black Velvet paint. The radiative effects of the radiometer being calibrated are modeled by a source positioned behind the chopper, reflecting energy off the back of the chopper blade. The energy source is a MINCO self-measuring heater button. Radiation from this heater is focused on the aperture with an IRTRAN-4 f/2 lens. A liquid-nitrogen-cooled absorbing blackbody is positioned to intercept this radiation during the on-cycle of the chopper.

CAVITY DESIGN

Geometry

There is much data in the literature on the emittance of blackbody cavities; however, the data is of very little use to this design task for two reasons:

a) The data is for straight cylindrical and conical holes without entrance lips.

b) The data is primarily hemispherical emittance, not directional emittance for small (10°) solid angles.

A lip can greatly improve the emittance of a fixed-length cavity, provided the walls are isothermal, by providing an increased length/diameter ratio which is the case in this low-temperature application.
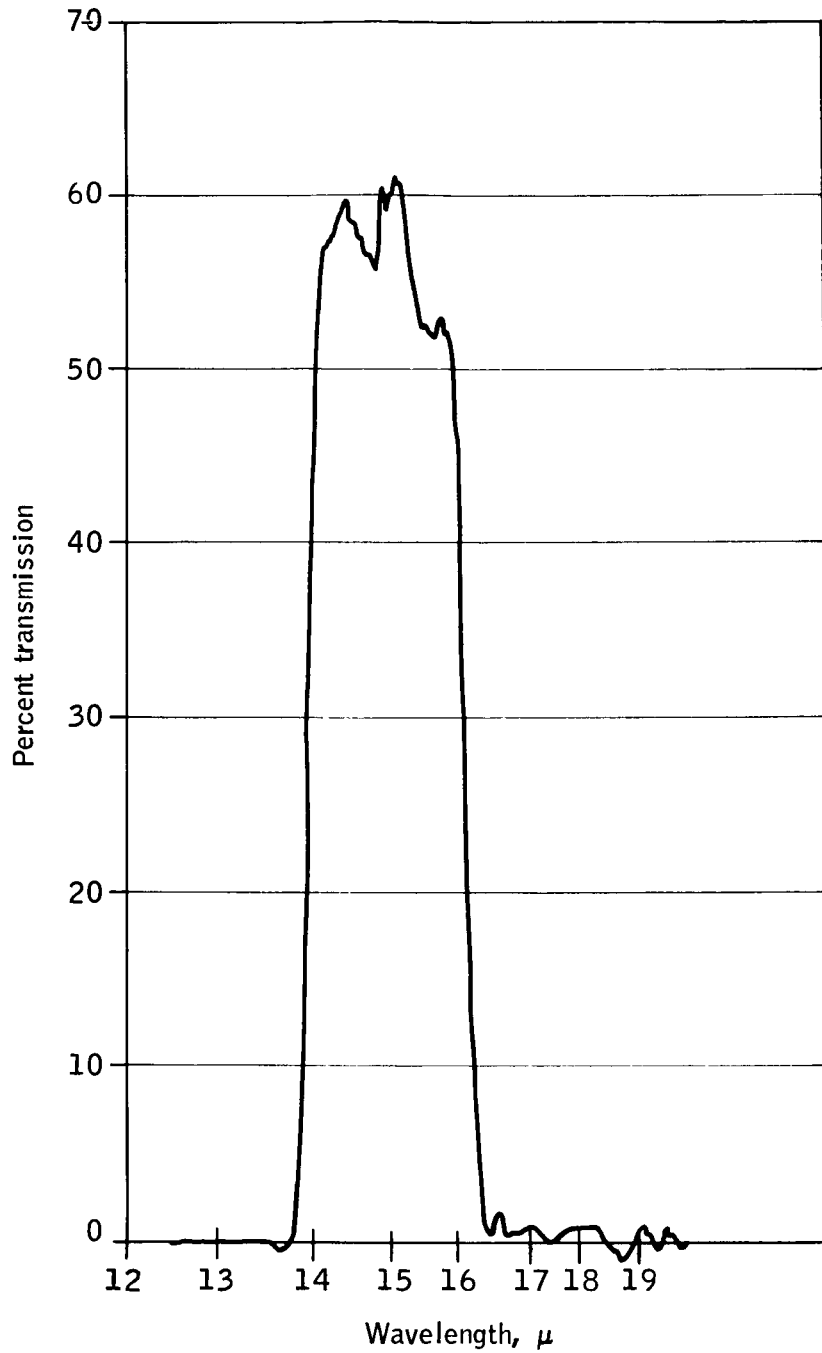
Figure 11.   Spectral Response of 14 to 16μ Filter

It is very plausible to have a high directional emittance near normal and at the same time not to have a high hemispherical emittance. Therefore, an independent evaluation of the blackbody geometry design was undertaken.

First, the interrelationship of reflectance values with directional emittance is considered.

The reflectance for a ray incident in the direction θ_1, ϕ_1 and reflected in the direction θ_2, ϕ_2 (see Figure 12) is defined as

$$\rho\ (\theta_1,\ \phi_1,\ \theta_2,\ \phi_2)$$

For hemispherical reflectance with directionally incident radiation, this expression becomes

$$\rho_i\ (\theta_1,\ \phi_1) = \int_0^{2\pi} \int_0^{2\pi} \rho\ (\theta_1,\ \phi_1,\ \theta_2,\ \phi_2)\ \sin\theta_2\ d\theta_2\ d\phi_2$$

In the following, the subscript i refers to the integration over the hemisphere.
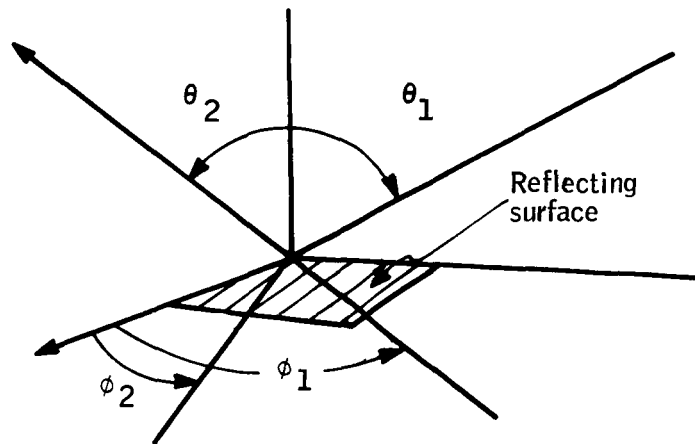
Figure 12. Geometry of Reflection

The Helmholtz reciprocity relationship states that the hemispherical reflectance for directionally incident energy $\rho_{i_2} (\theta_1, \phi_1)$ equals the directional reflectance for hemispherically incident energy $\rho_{i_1} (\theta_2, \phi_2)$. See Figure 13.

$$\rho_{i_2} (\theta_1, \phi_1) = \rho_{i_1} (\theta_2, \phi_2)$$
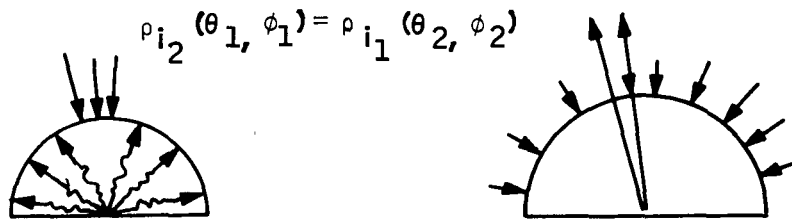
Figure 13. Reciprocity

Hemispherical reflectance for directionally incident energy is the ratio of energy reflected in all directions to that incident from only one direction when energy is incident from only one direction. Directional reflectance for hemispherically incident energy is the ratio of energy reflected in one direction to energy incident from the same direction when energy is incident from all directions (hemispherically).

This relationship is often used in radiation property measurements to equate one type of measurement to the other property. Next, the relationship between emissivity and reflectance is derived.

From conservation of energy incident on a surface from a single direction for an opaque surface

$$\tau_i (\theta, \phi) = 0$$

and

$$\rho_i (\theta, \phi) + \alpha (\theta, \phi) = 1.0$$

These relations hold for monochromatic energy as well;

$$\rho_{i_2} (\theta, \phi, \lambda) = \rho_{i_1} (\phi, \theta, \lambda)$$

and

$$\rho_i (\theta, \phi, \lambda) + \alpha (\theta, \phi, \lambda) = 1.0$$

26

From Kirchhoff's law,

$$\alpha \ (\theta, \ \phi, \lambda) \ = \ \varepsilon \ (\theta, \ \phi, \lambda)$$

Therefore,

$$\varepsilon \ (\theta, \ \phi, \lambda) \ = \ 1.0 - \rho_i \ (\theta, \ \phi, \lambda)$$

A way of determining the spectral directional emissivity, either experimentally or analytically, is to evaluate the proper reflectance value, either $\rho_{i_2} \ (\theta_1, \ \phi_1, \lambda)$ or $\rho_{i_1} \ (\theta_2, \ \phi_2, \lambda)$. The relations discussed above are illustrated in Figure 14.

Specularly reflecting coatings are known to generally produce higher emitting blackbody cavities than equivalent diffuse reflecting coatings. The use of specular surfaces and the reciprocity relationship permits evaluation of the directional emittance by ray tracing reflected energy. The hemispherical reflectance for directionally incident energy can be evaluated by ray tracing energy incident from a selected direction and determining the number of reflections the ray goes through before it emerges from the cavity.

The classical blackbody cavity (wide cylinder with a conical base and entrance lip) was found to be satisfactory ($\varepsilon_o > 0.9999$) provided the angle of the cone base was properly selected. Cone half-angles of 45 to 30° on the base cone are unacceptable because near-normal energy is reflected directly out after only two and three reflections, respectively.

$$\rho_i \ (\theta, \ \phi) \cdot H$$

$$\rho_i \ (\theta, \ \phi) \cdot H + \alpha(\theta, \ \phi) \cdot H + \tau_i \ (\theta, \ \phi) = H$$

$$\rho_i \ (\theta, \ \phi) + \alpha(\theta, \ \phi) + \tau_i \ (\theta, \ \phi) = 1$$

$$\alpha(\theta, \ \phi) \cdot H$$

$$\tau_i \ (\theta, \ \phi) \cdot H$$
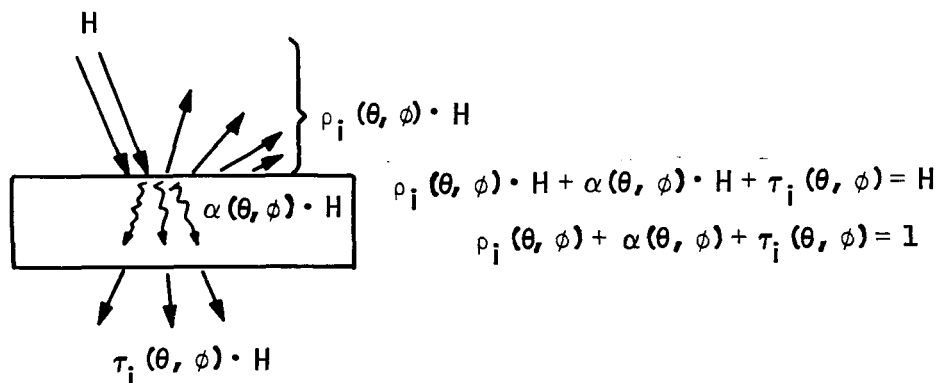
Note: This subscript i refers to hemispherical and the parameters θ and ϕ to direction.

Figure 14.   Conservation of Energy

The reason for discarding the classical blackbody design was concern of creating a small paint fillet at the apex of the cone which would reflect energy directly out the aperture on the first reflection. If the coating emittance were 0.90, a fillet of 1 mm^2 would cause an unacceptable emittance error. The goal here is to produce a blackbody with a directional emissivity greater than 0.9999. For this emittance, the area of the fillet causing single reflection out the aperture could be no larger than 0.1 mm^2.

Even more important than the emissivity error itself is the error caused by back reflection of radiance emanating from a warm radiometer. If a calibration point is being taken at low temperature (90°K), the 14 to 16μ energy incident on the blackbody aperture from a warm radiometer is 10^3 greater than the emission from the blackbody in the radiometer view angle. A blackbody reflectance of 10^{-3} (ε = 0.999) causes little error if the cavity reflects diffusely; that is, the reflected energy emerges from the cavity and goes in all directions because of random internal multiple reflections. For a diffuse reflection, less than 10^{-2} of the energy reflected out the aperture goes into the radiometer acceptance cone. However, if a significant portion of the cavity reflectance is a result of a single reflection, such as a paint fillet in the apex of the back surface, reflectance errors as high as 100 percent of the blackbody emission are conceivable.

To eliminate this potential problem, the blackbody cone is placed off-axis so the apex is not viewed directly by the radiometer. Simple ray traces on the classical blackbody cavity and the selected off-axis conical cavity are shown in Figures 15 and 16 respectively. A minimum of seven specular reflections occur for the 10° aperture cone in either geometry.
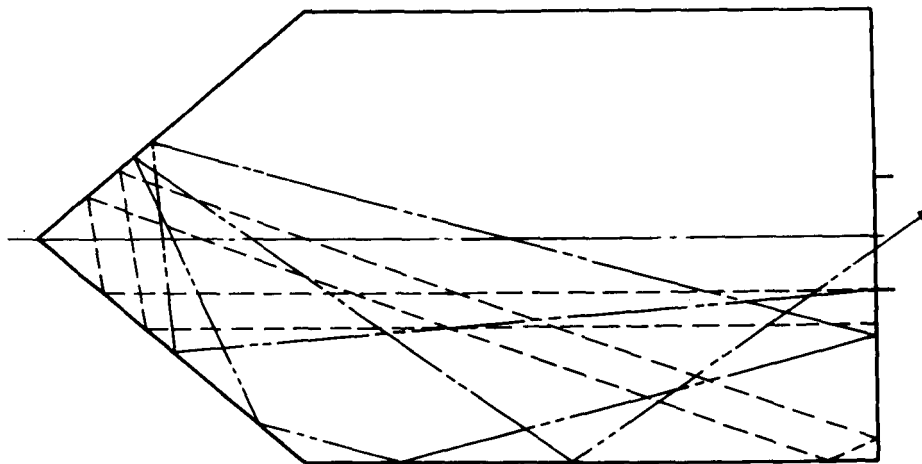
Figure 15. Ray Trace of Classical, Conical Blackbody
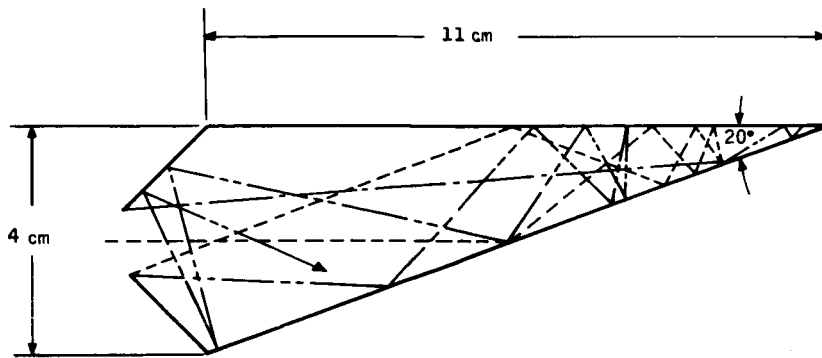
Figure 16. Ray Trace of Off-Axis Cone

Calculations were made to evaluate the blackbody directional emittance if the internal coating were diffuse. The following analysis is for the off-axis conical cavity shown in Figure 16. The cavity is described as three areas- the aperture is denoted by the subscript "a", the area on the back surface subtended by the 10° aperture cone is denoted by subscript "1", and all remaining area is denoted by subscript "2". The entire cavity surface "1" and "2" is denoted by subscript "b".

The shape factor from the aperture to area 1 can be evaluated by simple geometry ($F_{a-1} \approx 0.02$). This value was obtained by direct evaluation of the extremities of the surface, using Hammond's construction as described by Eckert in reference 6, and taking the mean of these values. Figure 17 shows the results of this construction.
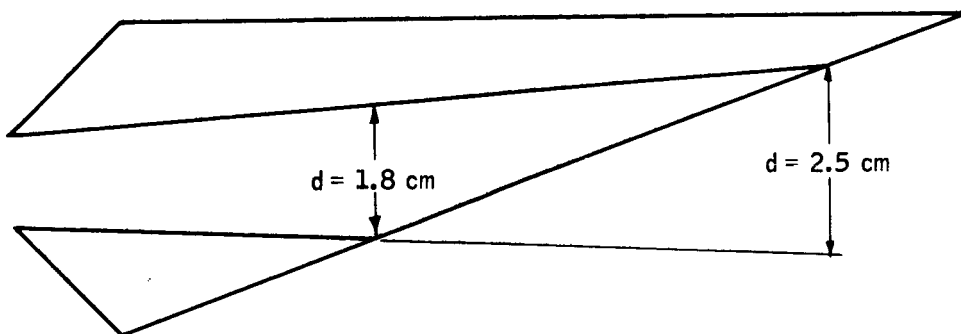
Figure 17. View Factor

The areas are evaluated by geometry as follows:

$$A_a \simeq 1.572 \text{ cm}^2$$

$$A_1 \simeq 8.12 \text{ cm}^2$$

$$A_2 \simeq 30.7 \text{ cm}^2$$

From reciprocity,

$$A_a F_{a-1} = A_1 F_{1-a}$$

and

$$F_{1-a} = \frac{A_a}{A_1} F_{a-1} \simeq 0.0039$$

Assuming that area 1 does not view itself, which is not entirely correct but a conservative assumption,

$$F_{1-2} = 1 - F_{1-a} \simeq 0.9961$$

From reciprocity again,

$$A_2 F_{2-1} = A_1 F_{1-2}$$

and

$$F_{2-1} = \frac{A_1}{A_2} F_{1-2} \simeq 0.258$$

It should be noted that if area 1 views itself with a shape factor of $1/4$, then

$$F_{2-1} \simeq 0.193$$

and

$$F_{a-2} = 1 - F_{a-1} = 0.98$$

From reciprocity again,

$$A_a F_{a-2} = A_2 F_{2-a}$$

and

$$F_{2-a} = \frac{A_a}{A_2} \; F_{a-2} \simeq 0.05$$

The shape factor between the entire blackbody cavity and the aperture is evaluated by

$$A_b \, F_{b-a} = A_a \, F_{a-b} = A_a \, (F_{a-1} + F_{a-2})$$

where

$$F_{b-a} = \frac{A_a}{A_1 + A_2} \; (F_{a-1} + F_{a-2}) \simeq 0.04$$

With these numbers the directional emittance of the blackbody cavity with a diffuse reflecting coating can now be evaluated. Two calculation procedures are used:

    a)   Assume totally diffuse energy is entering the aperture and evaluate the amount reflected out the aperture into the radiometer acceptance cone compared with that portion of the incident energy coming from the same cone.

    b)   Assume energy incident on the aperture from the radiometer acceptance angle and evaluate the energy reflected out the aperture in all directions.

First, the hemispherical reflectance for directionally incident energy $\rho_i(\theta, \phi, \lambda)$ is calculated. All the energy is incident on surface 1 so the energy escaping through the aperture upon the first internal reflection is $H(\theta, \phi, \lambda) \, \rho_\lambda F_{1-a}$, where $H(\theta, \phi, \lambda)$ is the incident energy, F_{1-a} is the shape factor from surface 1 to the aperture, and ρ_λ is the internal surface reflectance.

The energy reflected out the aperture on the second reflection is

$$H(\theta, \phi, \lambda) \, \rho_\lambda F_{1-2} \, \rho_\lambda \, F_{2-a} + H(\theta, \phi, \lambda) \, \rho_\lambda F_{1-1} \, \rho_\lambda F_{1-a}$$

These can be combined into a single term:

$$H(\theta, \phi, \lambda) \, \rho_\lambda^2 \, F_{b-a}$$

The energy reflected out the aperture on the third reflection can be estimated in similar manner:

$$H(\theta, \phi, \lambda) \, \rho_\lambda^3 \, F_{b-a}$$

Admittedly, the equations for the second and third reflections are simplifications of the true picture because the energy reflected onto surface 2 from surface 1 is not uniformly distributed over surface 2. However, the assumptions are conservative producing a high reflectance value:

$$\rho_i(\theta, \phi, \lambda) = \frac{H(\theta, \phi, \lambda)(\rho_\lambda F_{1-a} + \rho_\lambda^2 F_{b-a} + \rho_\lambda^3 F_{b-a} + \ldots)}{H(\theta, \phi, \lambda)}$$

$$= (0.10)(0.0039) +)0.01)(0.04) + (0.001)(0.004) + \cdots$$

$$= 0.0008$$

Therefore,

$$\epsilon(\theta, \phi, \lambda) = 0.9992$$

Now consider the analysis of $\rho(\theta, \phi, H, \lambda)$ for the same geometry with hemispherically incident energy.

Reflected energy emerging from the aperture into the 10° acceptance cone can only come from area 1. The first reflection produces

$$H_i(\lambda) F_{a-1} \rho_\lambda F'_{1-a}$$

Some of the energy reflected out the aperture from surface 1 is not reflected into the 10° acceptance cone, a result of the aperture having finite area;

$$F'_{1-a} < F_{1-a}$$
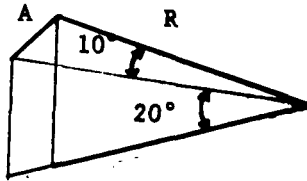
where

$$A' = A \sin 20°$$

and

$$F'_{1-a} = \frac{A'}{\pi R^2} = \frac{A \sin 20°}{\pi R^2} \approx \frac{\pi (R \sin 5°)^2 (\sin 20°)}{\pi R^2}$$

$$= 0.00259$$

32

The second reflection produces

$$H_i(\lambda)\,\rho_\lambda\,F_{a-2}\,F_{2-1}\,\rho_\lambda\,F'_{1-a} + H_i(\lambda)\,\rho_\lambda\,F_{a-1}\,F_{1-1}\,\rho_\lambda\,F'_{1-a}$$

These can be combined into a single term conservatively by assuming $F_{1-1} = F_{2-1}$:

$$H_i(\lambda)\,\rho_\lambda\,F_{2-1}\,\rho_\lambda\,F'_{1-a}$$

The third reflectance term is conservatively evaluated in the same way:

$$H_i(\lambda)\,\rho_\lambda^3\,F_{2-1}\,F'_{1-a}$$

The reflectance $\rho_i(\theta, \phi, \lambda)$ then becomes

$$\rho_i(\theta, \phi, \lambda) = \frac{H_i(\lambda)\,(F_{a-1}\,\rho_\lambda\,F'_{1-a} + \rho_\lambda^2\,F_{2-1}\,F'_{1-a} + \rho_\lambda^3\,F_{2-1}\,F'_{1-a} + \dots)}{F_{a-1}\,H_i(\lambda)}$$

$$= \frac{(0.02)(0.1)(0.0026) + (0.01)(0.25)(0.0026) + (0.001)(0.25)(0.0026)}{0.02}$$

$$= 0.00062$$

or

$$\epsilon(\theta, \phi, \lambda) = 0.9994$$

Cavity Coating

As shown above, specular coating yields a higher emittance cavity than a diffuse coating; hence a specular high-emittance paint was specified. The requirements for the coating are:

- High emittance in the 14 to 16μ range

- Vacuum operation

- Adhesion through repeated cycling from liquid nitrogen to room temperature.

Cat-a-lac black, a specular epoxy, was found to possess these properties. Reflectance was measured at 1, 5, 10, and 15μ. Data obtained is shown in Figure 18.
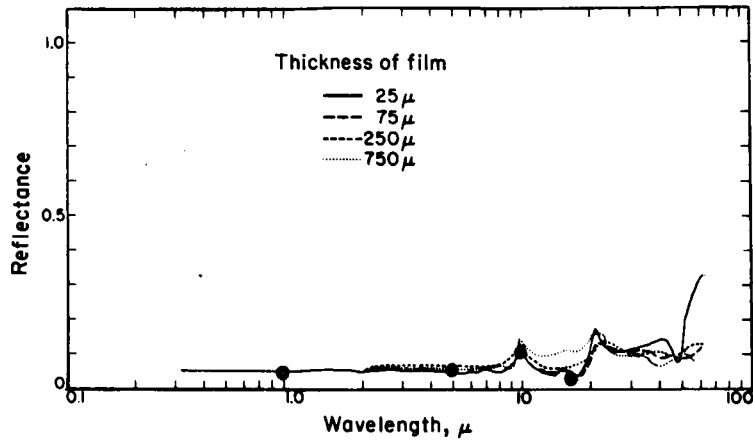
Figure 18. Reflectance of Cat-a-lac Epoxy Black Paint on Aluminum Substrate

The specularity of the reflectance at 2.75μ is indicated by data acquired from TRW thermal group in Redondo Beach, California (see Figure 19). This data is presented with a log scale and is much more specular than first seems. The off-specular peak is not surprising for such a coating. Specularity is expected to be more pronounced at 15μ, theoretically increasing as λ^4.

A sample of Cat-a-lac black was prepared on a flat plate for testing of adhesion. This sample was cycled 24 times between liquid-nitrogen and room temperature. A 1/16-inch grid was scribed on the surface, and the "Scotchtape" test applied. No problems were noted.

SUPPORTING SYSTEMS

The supporting systems are the chamber, devices to obtain motion in a vacuum, the thermal control system, simulated radiometer, and liquid-nitrogen shrouds.

A vacuum chamber is required because:

- Errors are introduced by transmission losses in atmosphere.

- There is coupling between the radiometer being calibrated and the source when operated in atmosphere.

- Convective heating of the system makes gradient control difficult.

The devices to obtain motion in a vacuum are required to permit the radiometric mapping of the source. Requirements are ±5° angular motion of the source, pivoted about its aperture, and vertical travel of at least 0.5 cm to permit mapping of the aperture surface.

The thermal control system provides a means to move the temperature of the source from one point to another rapidly and to control the temperature of the source within limits required for measurement during measurement intervals.

To determine whether there is significant interaction between the radiometer being calibrated and the source, a simulated radiometer, which provides a source of radiation with the characteristics of a full-scale radiometer, is required.

Liquid-nitrogen shrouding is used throughout to minimize background for the radiometric measurements.

Photographs of the completed system are shown in Figures 20 and 21.
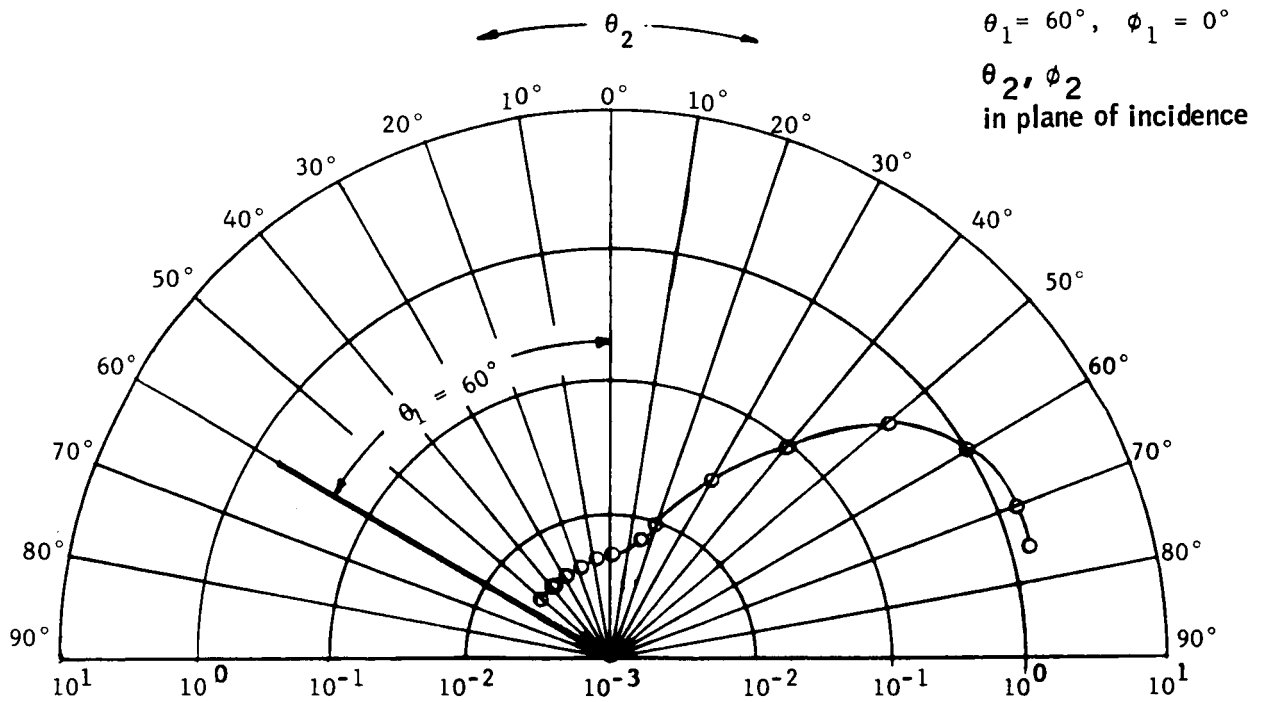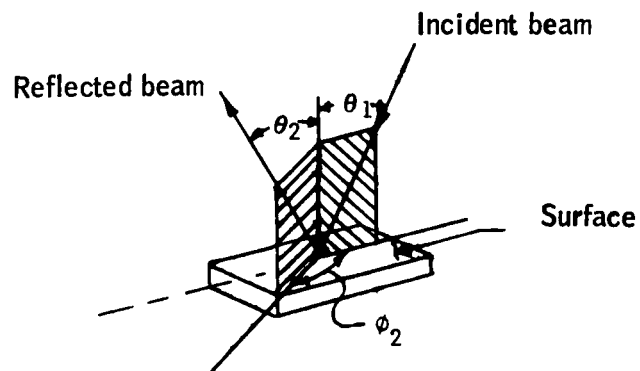
Figure 19. Directional Distribution of Reflected Radiation for Finch
Flat Black Paints (Cat-a-lac 463-1-8) at 2.75μ
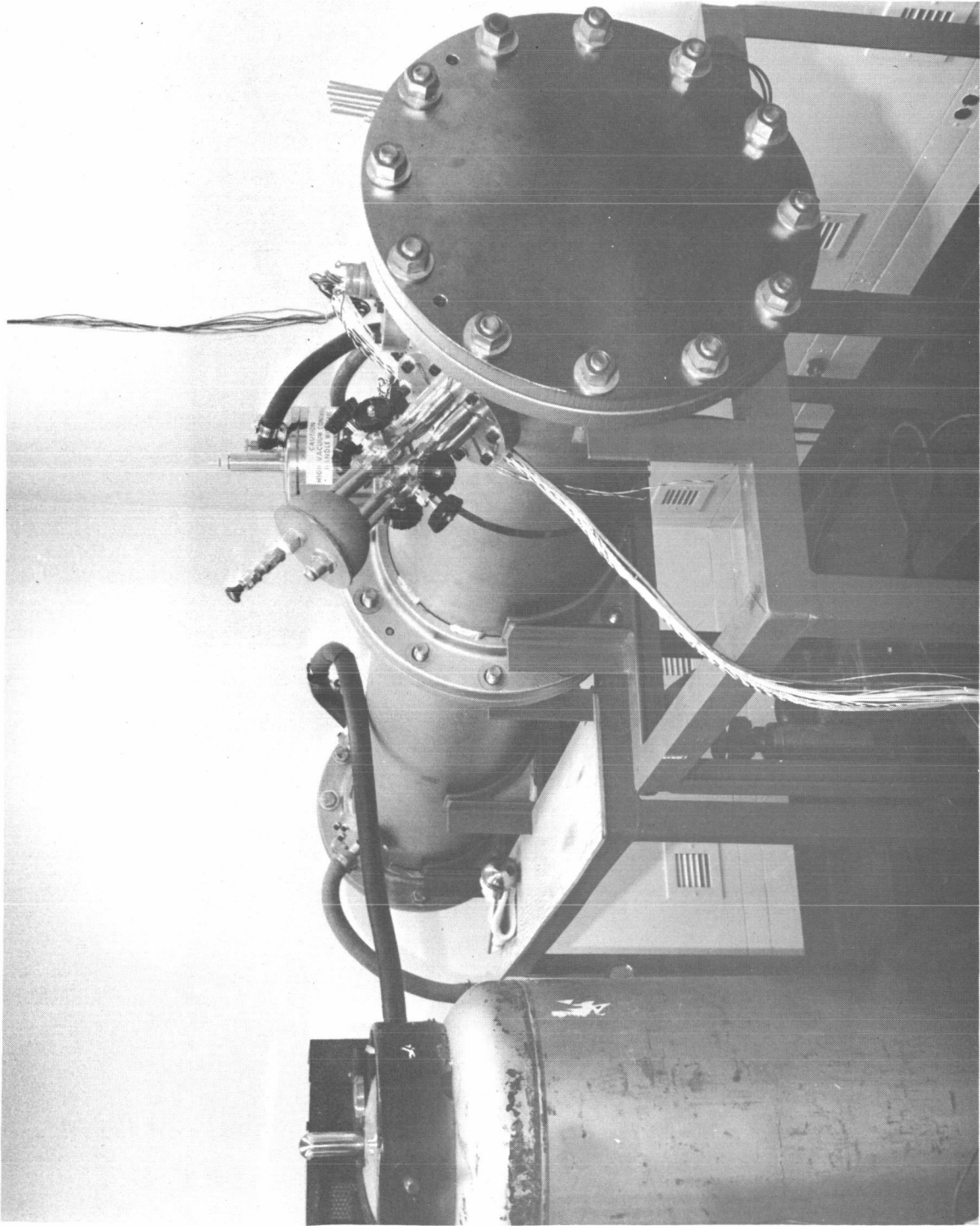
Figure 20. Assembled System - Left Side
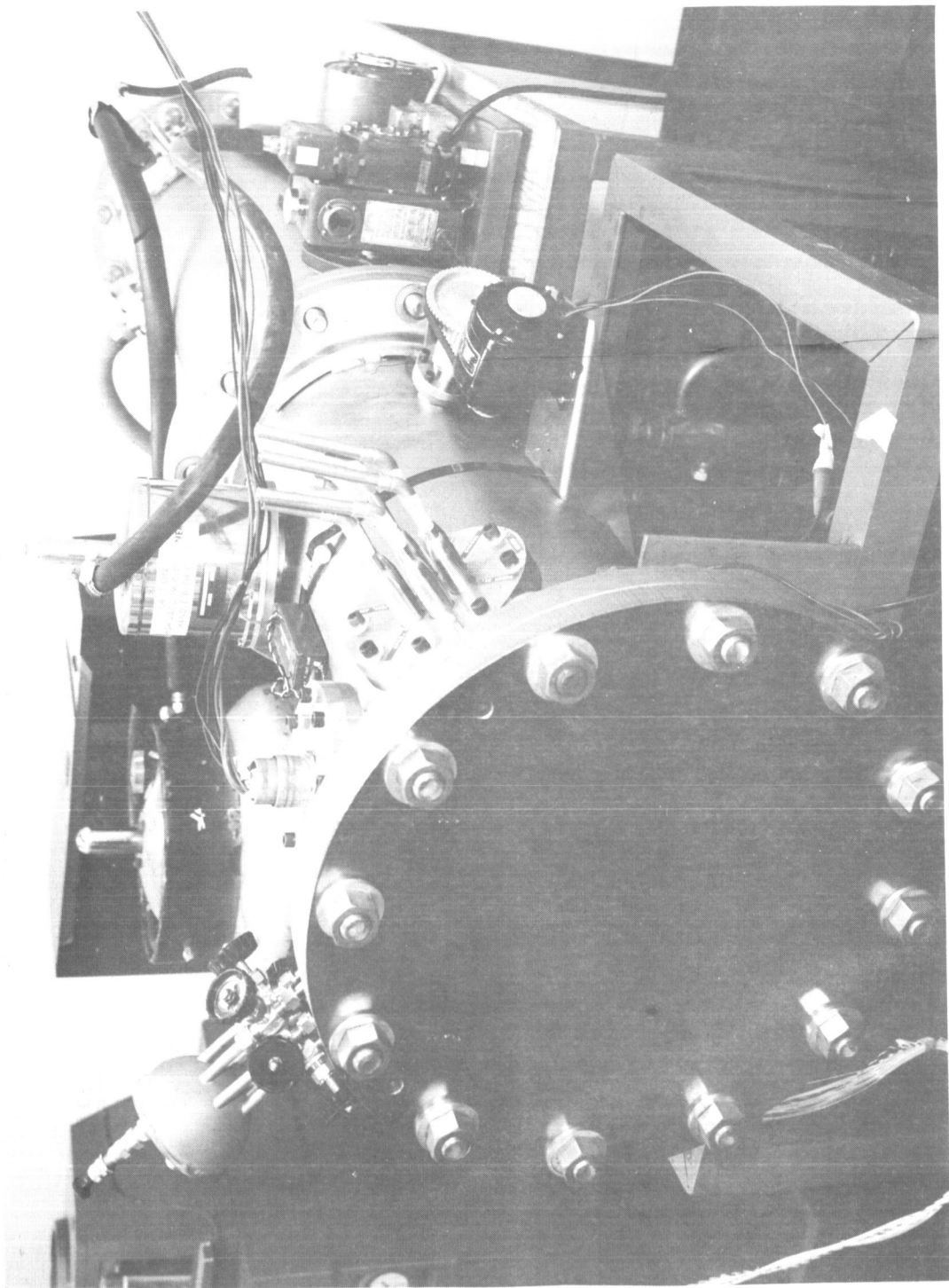
Figure 21. Assembled System – Right Side

Chamber

Due to the logistics of large liquid-nitrogen-cooled vacuum facilities and the difficulties involved in modification, a vacuum chamber was specially fabricated for this project. The chamber is 12 inches in diameter, two-section, fabricated of rolled steel and nickel plated. One section carries the source, chopper, baffle plates, liquid-nitrogen shrouds, and detector Dewar. This section is a complete source and is separable for flanging to a standard vacuum chamber. The other section carries a liquid-nitrogen shroud and an adjustable mirror and is used solely for the self-contained radiometer. Size was dictated by the availability of materials, particularly flanges. Vacuum seal on all flanges except the Dewar flange is obtained with aluminum wire gaskets.

The chamber sections each carry stationary liquid-nitrogen shrouds, separated from the outer walls by 1-inch fiberglass pads. The shrouds are fabricated of copper, with copper liquid-nitrogen lines soldered to the exterior. The interior is coated with 3M Black Velvet. A stationary liquid-nitrogen-cooled aperture baffle, which carries a wide-band filter and provides shrouding and first-stage aperture definition for the source-guard heater, is fabricated as a separate assembly to allow front access to the source. A removable two-part liquid-nitrogen-cooled baffle system is provided at the rear of the system to permit access to the source wiring. To provide full aperture definition over the range of motion, a liquid-nitrogen-cooled baffle plate is mounted on the front of the source-guard heater assembly on fiberglass rods and moves with the system. All liquid-nitrogen lines are flexible stainless bellows to permit motion of the system.

The source and guard heater system are movable as an assembly to permit mapping of the aperture by the self-contained radiometer. The system is supported on stainless-steel rods, and motion is obtained with external screw-drives through stainless-steel bellows. The screws are specially fabricated micrometer screws (40-thread, 0.025 inch per revolution). Rotation is obtained by mounting on yokes with stainless standoffs pivoted on fiberglass mounting pads. The plane of mounting is the entrance aperture. Rotation is accomplished by motion of the rear screw on a two-point lever. Mechanical gain of the system is 4:1. The relationship of screw position to angular position is given in Figure 22.

Source

The source is fabricated from commercial bus-bar copper. The cavity was machined by cutting the base of the system at the appropriate angle and then cutting the cavity on a lathe, with a specially constructed conical tool. After initial machining, a tool mark was noted visually in the cavity. The cavity was hand-dressed with a jeweler's file and wet-sanded. Final surface finish obtained was measured on a Taylor and Hobson Tallysurf surface finish measurement system. Finish was better than 50 microinches throughout (1/4-wave at 15μ is roughly 200 microinches). The front lip was separately machined and press-fit. The off-axis cavity, cut at an angle off the normal, yields an elliptical cross-section, while the lip has a circular cross-section. Mismatch of the two sections is a maximum of 0.001 inch.

Liquid-nitrogen cooling coils were soldered to the block. Heating (for temperature change only) is obtained from a press-fit sleeve coated with spray-on heater. Heater power is 100 W at 110 V ac. The source assembly is held in the guard heater assembly on fiberglass standoffs.
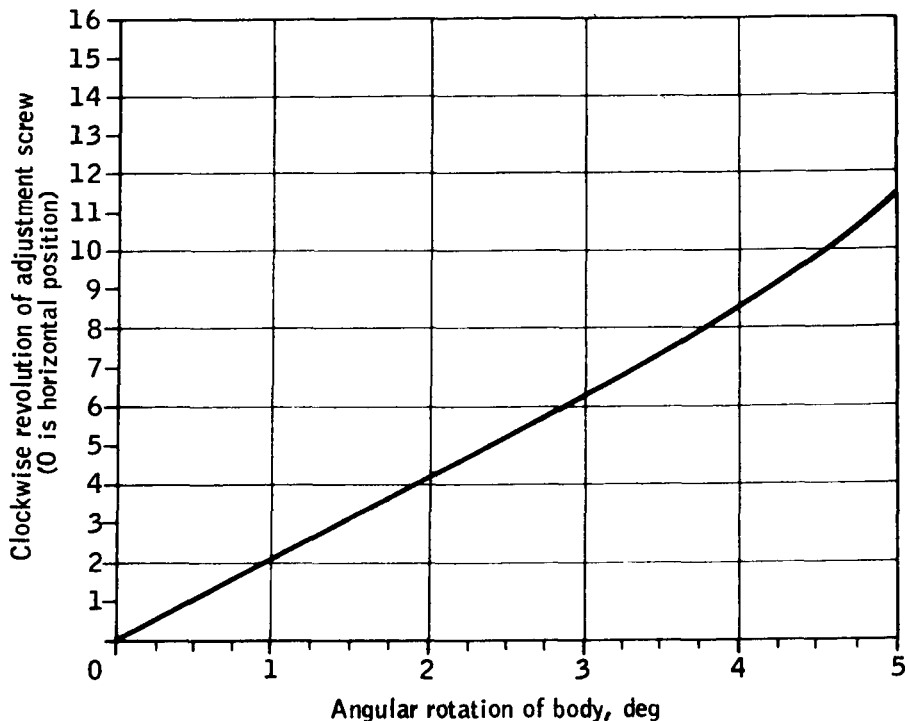
Figure 22. Aperture Scan Correlation Data

Guard Heater

For control during operation, a guard heater, controlled by a relay control amplifier operating from a temperature-sensing bridge, is used. The guard is fabricated in three sections-an aluminum inner sleeve, an aluminum liquid-nitrogen-line assembly, and an aluminum outer sleeve which is coated with spray-on heater. Aluminum end plates are coated with spray-on heater.

Thermal Control System

The final goal is a device usable in practice on a multiple-point calibration, which may be repeated several times. A period of the order of two to five minutes is adequate to read a Mueller bridge, if some prior knowledge of the temperature is available and the bridge is set up in advance. As a preliminary goal, it should not take longer than 20 to 30 minutes to change temperatures and to stabilize, giving roughly 16 calibration points per working day.

40

Since measurements are being made with precision in the range of 0.01°K, the requirement on the source is that the drift during a measurement be significantly less than 0.01°C or the slope of the temperature-time curve be less than 0.01°C/5 minutes.

The other major requirement on the heater is the relation of the thermometer measurement to the temperature of the cavity. Again, there cannot be gradients greater than approximately 0.01°C between the thermometer and the source.

<div align="center">
Source Time Constant and
Temperature Control
</div>

Preliminary calculations showed that only two design approaches to the temperature control of the source had potential for reducing both temperature gradients and variations in time down to the 0.01°C level. One approach consists of thermally isolating the source from the chamber to as high a degree as possible, thus enabling the source time constant to be hundreds of hours. Active heating and cooling of the block would only be used to change its temperature level. The second approach would consist of surrounding the block with a lightweight temperature-controlled guard heater. Thermal insulation would still be required but would not be as critical. Active heating and cooling of both block and guard are used to change temperature levels; hence, there is not large heat flow during a measurement cycle. A control heater on the guard cycles the guard about a selected control temperature. This control can be relatively coarse, since the function of the guard heater is to reduce the gradient between source and sink.

Analysis showed that the highly insulated source design (no guard heater) can be pushed to a time constant of approximately 800 hours. This means that the block temperature varies less than 0.01°C in the time required to take a data point under all conditions. The block would be wrapped in multifoil insulation, suspended by fiberglass monofilament lines, and connected to power and instrumentation with spiral-wound leads having the greatest thermal resistance possible. Heater power to a heater on the block would be applied to change the block temperature, and calculations indicate that a stabilization time of several minutes after power cutoff is sufficient to eliminate temperature gradients. However, heater power during temperature level changes would also be transferred into the wrapped insulation, and calculations indicate that several hours might be required for this effect to be extinguished. Thus, unreasonable lengths of time would be needed between data points.

The design incorporating a guard heater was analyzed. The analysis showed that the multifoil insulation can be eliminated. For example, a 15-pound copper block was assumed to be completely surrounded by a 4.4-pound polished aluminum guard except for the blackbody aperture. A 10W on-off heater on the guard was assumed to be controlled to ±1°C by a sensor on the guard. The block temperature was found to cycle between ±0.004°C. Conduction between the block and guard (leads, lines) as well as radiation was considered in the analysis. Heat loss from the aperture and the outside of the guard was to a -200°C environment. See Figures 23 and 24.

2.2# al .guard
15.0# cu. source
1 cm aperture
$K_{G-S} = 0.0145$ W/°C
$K_{G-0} = 0.0296$ W/°C
$T_0 = -200$°C
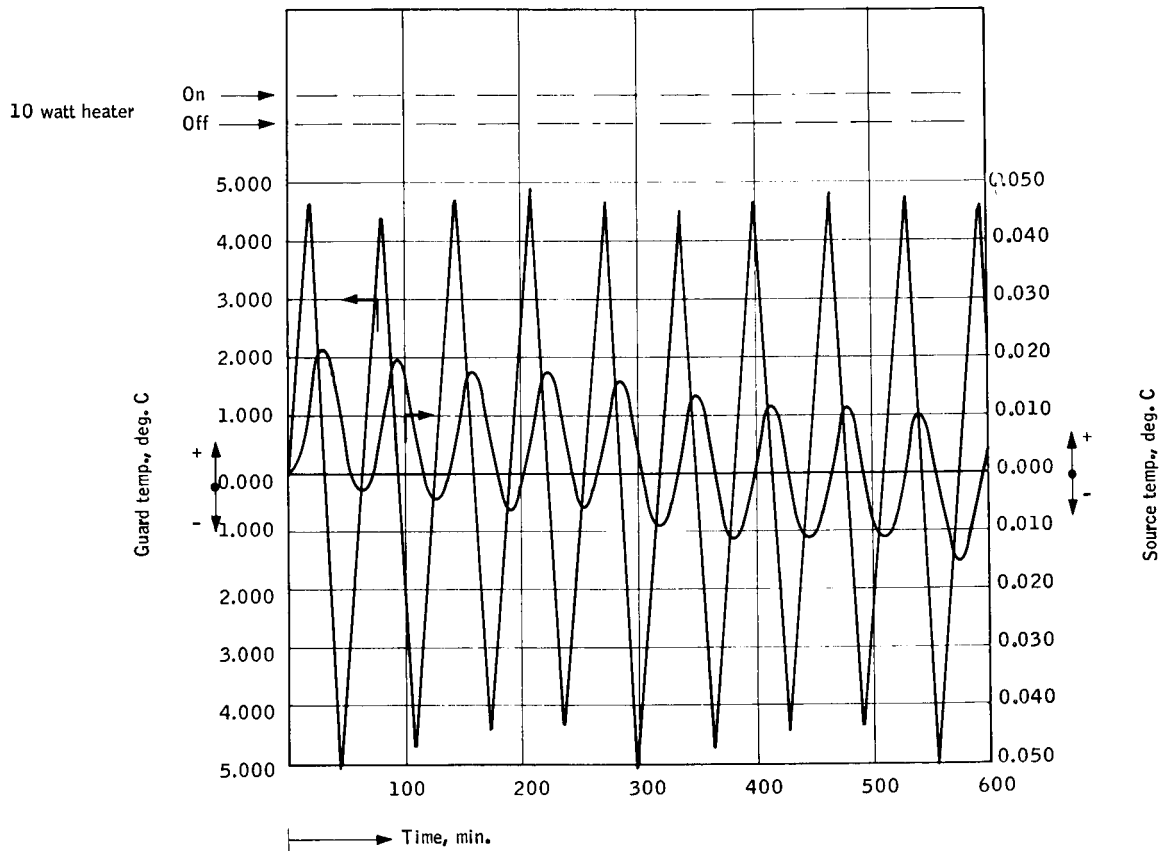
Figure 23. Temperature Control with Guard Heater (Cases 1 and 2)
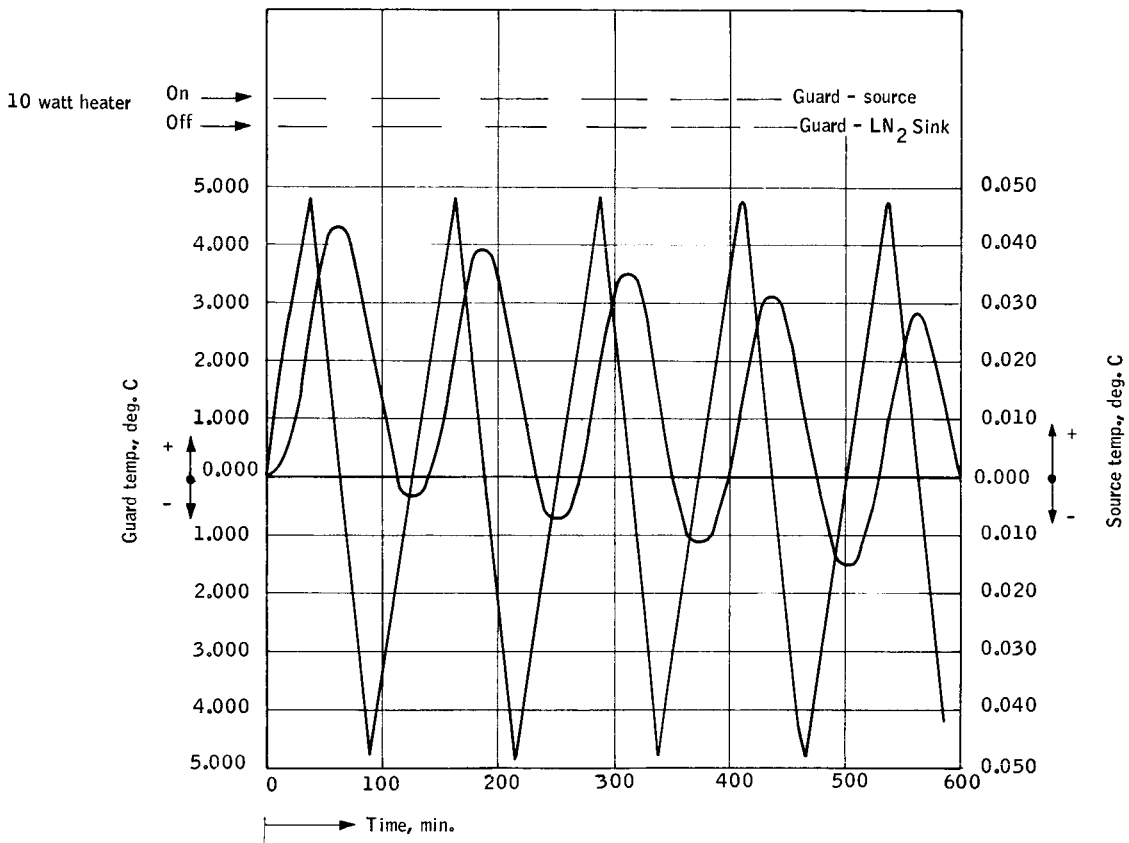
Figure 24. Temperature Control with Guard Heater (Cases 1 and 2)

The above concept was, therefore, adopted as most suitable for this application. The only disadvantages are the extra complexity of a heater/sensor and the need for coolant lines to the guard as well as the block.

Thermal Control System Electronics

Temperature sensing for control uses MINCO nickel-iron resistance thermometers with nominal resistance of 661 ohms at 20°C. The system uses a Thermo-electric model No. 70298 relay control amplifier. Table 2 gives the nominal calibration for these thermometers.

Three bridge configurations were investigated for the control system. These are shown in Figure 25.

The configuration shown in Figure 25a controls on temperature differential between source and guard. In practice, this system gives reasonable control, particularly at high temperatures, and is simple to balance. A downward drift of the order of 0.01°C per one to two minutes was obtained at low temperatures.

In an attempt to counteract this drift, the bridge shown in Figure 25b was installed. This bridge controls on both absolute and differential temperature. The drift found above was accentuated and balance of this bridge is extremely difficult.

On the assumption that the guard heater did not possess adequate power, an attempt was made to correct the drift by applying the control circuit to the source heater, using a Variac to reduce the power of this heater. It was not possible to obtain sufficiently fine control to allow reading of the Mueller bridge with direct heating of the source.

The third approach, shown in Figure 25c, gives control of the source absolute temperature and is the standard heater control circuit.

During the series of experiments with the system described above, two effects were noted. First, it was found that the source temperature was drifting upward when the source was near room temperature and the balance of the system was at liquid-nitrogen temperatures, indicating a severe thermal short to the outside world. After investigation it was determined that the liquid-nitrogen lines to the source which were not in use had iced. The lines were cleared by heating the source and applying vacuum to the lines.

Secondly, the system after initial assembly did not exhibit a thermal gradient. However, after a teardown to correct mechanical deficiencies, a gradient of the order of tens of millidegrees was obtained. The system was examined and the wiring harness redone to avoid coupling of active liquid-nitrogen lines to the block.

44

TABLE 2. RESISTANCE RATIO-FAHRENHEIT

NOMINAL RESISTANCE AND RATIO VALUES
FOR MINCO SENSORS HAVING MS-1 ELEMENT MATERIAL

Range: -330°F to +610°F.

Ratio: (Based on 32°F) $R_T = R_{32} \times RATIO$

Note: Due to difference in structure, the values may vary slightly with different types of sensors. Correction factors will be supplied with sensor types which vary from this nominal table. See catalog sheet for applicable temperature or operating range.

RES.(Ω)	T (°F)	RATIO	RES.(Ω)	T (°F)	RATIO	RES.(Ω)	T (°F)	RATIO	RES.(Ω)	T (°F)	RATIO
242.05	-330	0.40075									
244.41	-325	0.40465	456.64	-75	0.75603	801.64	150	1.32722	1312.28	400	2.17265
246.84	-320	0.40868	462.77	-70	0.76618	810.63	155	1.34210	1323.77	405	2.19167
249.35	-315	0.41283	468.98	-65	0.77645	819.67	160	1.35707	1335.31	410	2.21078
251.93	-310	0.41710	475.26	-60	0.78685	828.76	165	1.37212	1346.89	415	2.22995
254.58	-305	0.42149	481.61	-55	0.79737	837.90	170	1.38725	1358.53	420	2.24922
257.31	-300	0.42601	488.04	-50	0.80801	847.09	175	1.40247	1370.22	425	2.26858
260.11	-295	0.43065	494.54	-45	0.81878	856.33	180	1.41777	1381.96	430	2.28801
262.99	-290	0.43541	501.12	-40	0.82967	865.62	185	1.43315	1393.75	435	2.30753
265.94	-285	0.44029	507.77	-35	0.84068	874.96	190	1.44861	1405.59	440	2.32714
268.96	-280	0.44530	514.49	-30	0.85181	884.35	195	1.46416	1417.48	445	2.34682
272.06	-275	0.45043	521.29	-25	0.86306	893.79	200	1.47979	1429.42	450	2.36659
275.23	-270	0.45568	528.16	-20	0.87443	903.28	205	1.49550	1441.41	455	2.38644
278.47	-265	0.46105	535.10	-15	0.88593	912.82	210	1.51129	1453.45	460	2.40637
281.80	-260	0.46655	542.12	-10	0.89755	922.40	215	1.52716	1465.54	465	2.42639
285.19	-255	0.47217	549.21	-5	0.90929	932.03	220	1.54310	1477.67	470	2.44648
288.66	-250	0.47791	556.38	0	0.92116	941.72	225	1.55914	1489.85	475	2.46664
292.20	-245	0.48377	563.62	5	0.93315	951.46	230	1.57526	1502.08	480	2.48689
295.82	-240	0.48976	570.94	10	0.94526	961.25	235	1.59147	1514.36	485	2.50722
299.51	-235	0.49587	578.32	15	0.95749	971.09	240	1.60776	1526.69	490	2.52763
303.27	-230	0.50210	585.78	20	0.96984	980.98	245	1.62414	1539.08	495	2.54815
			593.32	25	0.98232						
307.10	-225	0.50845				990.92	250	1.64060	1551.52	500	2.56874
311.02	-220	0.51493	600.93	30	0.99492	1000.91	255	1.65714	1564.00	505	2.58940
315.00	-215	0.52153				1010.94	260	1.67374	1576.53	510	2.61015
319.06	-210	0.52825	604.00	32	1.00000	1021.02	265	1.69043	1589.12	515	2.63099
323.19	-205	0.53509				1031.16	270	1.70722	1601.76	520	2.65192
			608.67	35	1.00773						
327.40	-200	0.54206	616.52	40	1.02073	1041.35	275	1.72409	1614.45	525	2.67293
331.69	-195	0.54915	624.41	45	1.03379	1051.59	280	1.74104	1627.19	530	2.69402
336.04	-190	0.55636				1061.88	285	1.75808	1639.98	535	2.71520
340.47	-185	0.56369	632.35	50	1.04693	1072.21	290	1.77519	1652.82	540	2.73646
344.97	-180	0.57115	640.34	55	1.06016	1082.60	295	1.79239	1665.70	545	2.75778
			648.38	60	1.07348						
349.55	-175	0.57873	656.47	65	1.08687	1093.04	300	1.80967	1678.63	550	2.77919
354.20	-170	0.58643	664.61	70	1.10035	1103.53	305	1.82703	1691.61	555	2.80068
358.93	-165	0.59425				1114.06	310	1.84447	1704.65	560	2.82227
363.73	-160	0.60220	672.80	75	1.11391	1124.65	315	1.86200	1717.74	565	2.84394
368.60	-155	0.61027	681.04	80	1.12755	1135.29	320	1.87962	1730.88	570	2.86570
			689.33	85	1.14127						
373.55	-150	0.61846	697.67	90	1.15508	1145.98	325	1.89732	1744.07	575	2.88753
378.57	-145	0.62677	706.06	95	1.16897	1156.72	330	1.91510	1757.31	580	2.90945
383.67	-140	0.63521				1167.51	335	1.93296	1770.59	585	2.93144
388.84	-135	0.64377	714.50	100	1.18295	1178.35	340	1.95091	1783.91	590	2.95349
394.08	-130	0.65245	722.99	105	1.19700	1189.24	345	1.96894	1797.29	595	2.97565
			731.53	110	1.21114						
399.40	-125	0.66125	740.12	115	1.22536	1200.18	350	1.98705	1810.72	600	2.99788
404.79	-120	0.67010	748.76	120	1.23967	1211.17	355	2.00525	1824.20	605	3.02020
410.25	-115	0.67923				1222.20	360	2.02351	1837.73	610	3.04260
415.79	-110	0.68840	757.45	125	1.25406	1233.28	365	2.04185			
421.40	-105	0.69769	766.19	130	1.26853	1244.41	370	2.06028			
			774.97	135	1.28307						
427.09	-100	0.70711	783.81	140	1.29770	1255.59	375	2.07879			
432.86	-95	0.71665	792.70	145	1.31242	1266.82	380	2.09739			
438.69	-90	0.72631				1278.11	385	2.11608			
444.60	-85	0.73609				1289.45	390	2.13485			
450.58	-80	0.74600				1300.84	395	2.15371			

a. Control of temperature differential
   between source and guard

b. Control of absolute and differential
   temperatures

c. Control of absolute source temperature

Figure 25. Bridge Configurations for Thermal Control

Simulated Radiometer

One of the areas to be investigated with the calibration system is the interaction of the radiometer being calibrated with the calibration source. The nominal operating temperature of the HDS radiometer is in the range 200 to 300°K. As noted above, the source must operate down to 100°K. There is then a considerable net radiative heat flow from the radiometer to the calibration source. Although a perfect blackbody is by definition a perfect absorber, it is clear that conditions can occur (e. g., coating nonuniformities) under which absorption of radiation might force gradients in the source. Accordingly, a simulation of the radiometer radiation is included in the calibration system.

To obtain a set of measurements which reflect the source characteristics only with no other effects commingled, the self-contained radiometer mirror is cooled to liquid-nitrogen temperatures and a wide-band filter is installed to block emission of the Dewar window. A separate source is included to simulate the effects of the radiometer which is being calibrated. The source is a MINCO self-measuring heater button, 3/4-inch in diameter. This is installed in a folded optical system, using a Kodak IRTRAN-4 lens to obtain an image of this source at the entrance aperture. With this imaging, the temperature (and hence the wavelength function) is identical to the HDS radiometer. The device is installed behind the chopper and uses the back of the chopper blade as a folding element. During the on-cycle of the chopper, this system radiates through the chopper and is collected by an absorbing cavity cooled to liquid-nitrogen temperatures.

EXPERIMENTS

A series of experiments was conducted during the design and construction period.

These tests were designed to determine:

 a) Whether the split ring-leaf spring thermometer carrier assembly generated sufficient pressure to change thermometer calibration

 b) The conductance of the thermometer carrier assembly

 c) Block thermal gradients.

TEST PLAN

A test procedure was devised to ensure that all pertinent items are tested and to provide an estimate of the time and facilities required for testing.

Preliminary Testing and Set-up

Before final assembly of the system, checks of system integrity were made. These tests were:

 a) With no vacuum or cooling required

  ● Helium leak test - Source and guard liquid-nitrogen connections.

  ● Source positioning mechanisms - Screw-jack calibrations for source vertical position and angular position; source installed in chamber.

  ● Cavity coating, visual inspection - Surface roughness gage before installation of front piece.

  ● Preliminary radiometer focus and alignment - Using eyepiece in Dewar position and visible source at source position.

 b) Vacuum and/or cooling required

  ● Shroud and chamber outgassing.

  ● Chamber leak-testing, mass spectrometer leak detector - Both at room temperature and with cooled shroud.

- Integrity of source and baffle liquid-nitrogen flow paths (helium leak test).

- Source and guard heater operation.

- Check of source - Guard heater thermal time constant.

- Thermometer tracking - Ensure that thermometers after calibration track one another.

- Measurements of temperature at critical points - Chamber shroud, chamber wall, Dewar, radiometer mirror, liquid-nitrogen baffle plate, aperture baffle.

Preparation (to be performed before each test sequence and/or after any system repairs) is as follows:

Step number	Operation
1	Fill liquid helium Dewar. Verify radiometer operation by observing output from preamp on scope. System should show high-amplitude noise when observing room-temperature cavity (may be saturated).
2	Verify thermometer operation. Check thermometers against each other.
3	Verify source heater operation. Use short turn-on and monitor thermometer output and source temperature sensors.
4	Verify guard heater operation. Monitor guard temperature sensors.
5	Seal chamber. Leak test if required.
6	Pump down.
7	Introduce liquid nitrogen into chamber baffles and source. Sequence is: cool baffles; heat source for outgassing; cool source. Allow sufficient time for temperature stabilization. (Baffle guard thermal sensors and source thermometry show steady-state conditions and shroud outlet is liquid nitrogen.)
8	Turn on chopper motor. Examine waveform of preamp output on scope as a check for blade

8 (Cont.)	temperature anomalies. Record output of low-pass filter and source thermometry to establish background and system noise level.
9	Turn on source heater and drive the source to a high-temperature point. Turn on controller and stabilize temperature. Examine thermometer outputs for equivalence. Verify thermal time constant of source at this temperature.
10	Put preamp output on scope. Screw-jack the source vertically until output begins to fall off. The radiometer detector should then be straddling an edge. Double check against position calibration. Adjust mirror until peak output is obtained. Using small motions, iterate this adjustment until the sharpest energy drop at edge is obtained. The system is now in focus at temperature.
11	Step scan the mirror across the aperture normal to direction of travel of the source; step the source through its vertical travel at each step of mirror scan. Determine source centerline and center.
12	With system focused at center of the aperture, put preamp output on scope. Waveform will be analyzed for effective duty cycle and will be examined for chopper speed stabilization and waveform anomalies.

Analyze data obtained before proceeding with source testing. This data contains significant information regarding cavity gradient structure, emission gradients of the shroud, effectiveness of baffling, and radiometer performance, and these items should be verified.

TEST

Gonioradiometric Test

With system at center established above, and using rear screw-jack only, move screw-jack.

Repeat these measurements at 1° intervals through +5°, then swing through -5° and back to center in one-turn steps. These measurements are a set of gonioradiometric measurements for this position.

50

Source Aperture Scan

Using both screw-jacks, move source vertically 1 turn upward. Repeat the gonioradiometric tests above. Step the source at 1-mm intervals to the edge and back to the bottom edge, repeating the gonioradiometric measurement at each position.

Break the vacuum; rotate the source 90° in the split-ring holder.

Repeat the preparation described in steps 1 through 13.

Repeat the gonioradiometric test and source aperture scan sequence.

External Influence

Energize simulated radiometer at 200°K.

Repeat the preparation described in steps 1 through 13.

Repeat the gonioradiometric test and source aperture scan sequence.

Energize simulated radiometer at 300°K.

Repeat the preparation described in steps 1 through 13.

Repeat the gonioradiometric test and source aperture scan sequence.

Thermometer Testing

Preliminary checkout. -- A liquid-nitrogen bath was prepared and the thermometers checked under three conditions: bare, with their carriers, and with the thermometers and carriers installed in a copper block. The primary purpose of this testing was to determine whether the carriers affected the thermometer resistance. An unexpected difficulty was encountered in that a liquid-nitrogen bath is unstable and stratified; hence, conditions could not be repeated within the 0.01° K necessary to make a definite statement regarding the effect of the carriers upon the thermometers. The only point that could be verified was that the carriers certainly do not overstress the thermometer; a calibration at the ice point agreed within 0.001° K with REC's calibration after two days of alternate immersion of the thermometers and carriers in liquid nitrogen.

An attempt was made to verify the thermal conductance of the beryllium-copper carrier assembly. A copper block was fabricated which allowed immersion of one thermometer in liquid-nitrogen and held the other above the liquid-nitrogen surface. Lead configurations were maintained as similar as possible. The assembly was calibrated by immersing both thermometers

in liquid nitrogen. A difference of the order of 0.01° K was obtained as a base point. The assembly was then immersed such that one thermometer was in air, the other in liquid-nitrogen. A temperature difference of the order of 0.4° K was obtained. This difference is sufficiently large that convective heating of the thermometer in air was suspected.

An assembly which is capable of evacuation was prepared. The details are shown in Figure 26.
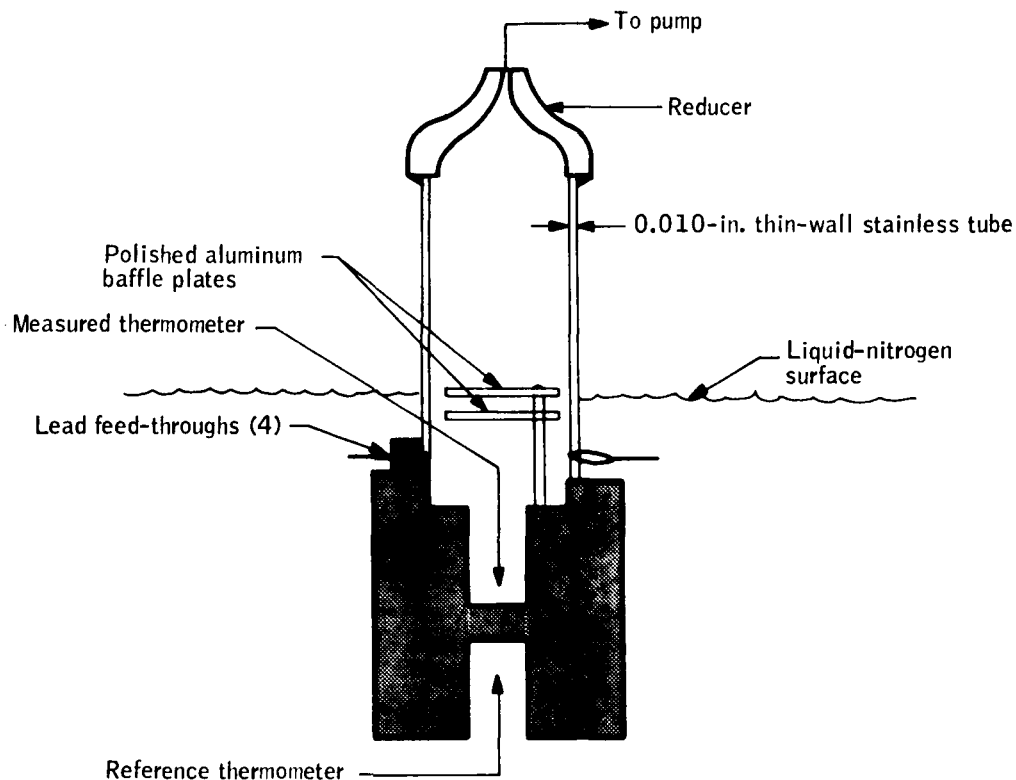
Figure 26. Conductance Measurement Apparatus

A copper block was machined to accept two thermometers. The thermometer and carrier whose conductance is to be measured is inserted in the top of the block and the four platinum leads taken out through vacuum feed-throughs. A second thermometer and carrier is installed in the base of the block. Leads for both thermometers are heat-stationed by wrapping on the block. A thin-wall stainless tube is soldered to the copper block above the feed-throughs, and a reducer is soldered to the thin-wall tubing to accept a vacuum hose. The block is immersed in liquid-nitrogen above the feed-throughs, ensuring that all leads are immersed in liquid nitrogen. The function of the thin-wall

tubing is conductive isolation of the upper surface of the block. A cold-baffle assembly is incorporated in the stainless tubing and is tied thermally to the copper block through an aluminum post to decouple the thermometer radiatively from the vacuum system.

Three experiments were performed with this set-up. First, the temperatures of both thermometers were measured after reaching bath stabilization. This is a simultaneous check on lead conduction and carrier thermal conductance and does not isolate carrier conductance. If a negligible temperature difference is obtained, either the lead thermal conductance is negligible or the carrier thermal conductance is high, or both. If a significant temperature difference is obtained, either lead conductance is high or carrier conductance is low, or both. There is no way in which the effects of lead conductance and carrier conductance can be separated with a simple temperature measurement. However, if negligible differences are obtained, and, if the lead conductance has been accurately represented, this is substantiating evidence to support the conclusion that the thermal conductivity of the carrier is adequate.

To isolate further the variables, it was proposed that the thermometer in vacuum be self-heated with a sufficient current so that any significant thermal resistance will cause a temperature rise in this thermometer. In this application millidegree accuracy is not sought, only sufficient accuracy to establish (say within 10 to 20 percent) the thermal conductance of the beryllium-copper/copper interface is of interest. For this degree of accuracy, the copper block can be assumed to represent a thermal short to the liquid-nitrogen bath. With this assumption, measurement of the temperature rise of the thermometer in vacuum over the temperature in the liquid-nitrogen bath with the same current is a direct measure of conductance.

Carrier conductance. -- The assembly shown in Figure 26 was completed and leak-checked. The effects of carrier conductance were experimentally determined.

Test no. 1: The system was immersed in liquid nitrogen. Without pumping, high drift rates and temperature differences of the two thermometers of the order of tenths of a degree were noted. After turning on the pump and allowing the system to stabilize, the following results were obtained:

Test date: 8 November 1967

Thermometer	Run number			
	1	2	3	4
No. 631 (in liquid-nitrogen) Temp., °K	77.2760	77.27466	77.28597	77.29680
No. 633 (in vacuum) Temp., °K	77.2615	77.25701	77.27014	77.27376
Temperature difference, °K	0.0145	0.01765	0.01583	0.023

The system was removed from the bath, and the thermometer carrier rotated 90°. The following results were obtained.

Test date: 10 November 1967 (All
runs over a five-minute interval)

Thermometer	Temperature, °K
No. 631	77.2978
No. 633	77.2877
Temperature difference	0.0101

Test no. 2: To obtain a base point, an assembly which allows both thermometers to be immersed in liquid nitrogen in a copper stabilizing block was used (Figure 27). With both thermometers immersed, the following results were obtained:

Test date: 10 November 1967

Thermometer	Temperature, °K
No. 633	77.2349
No. 631	77.2343
Temperature difference	0.0006

54
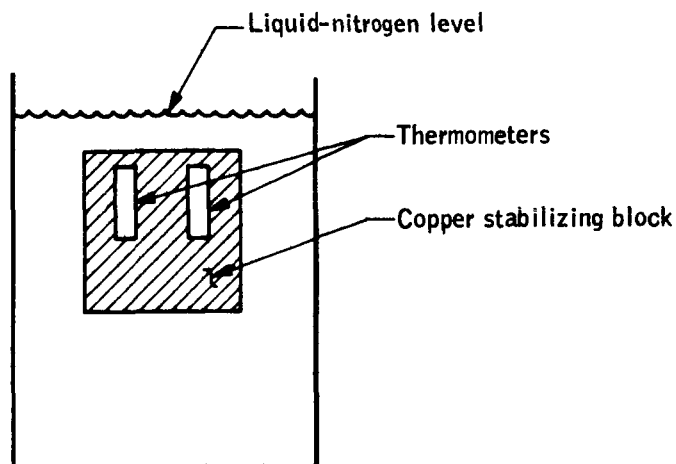
Figure 27. Stabilizing Block Assembly

Test no. 3: Carrier conductance was directly measured by self-heating both thermometers in the apparatus shown in Figure 26. Twenty mA were applied to each thermometer, giving 2 mW of I^2R heating (nominal resistance at liquid nitrogen is 5 ohms). The following results were obtained:

Thermometer	Temperature, °K	Current, mA
No. 631 (in liquid-nitrogen)	77.35067	2
	77.38189	20
Temperature difference	0.03122	
No. 633 (in vacuum)	77.35208	2
	77.42054	20
Temperature difference	0.06786	

Assuming the liquid nitrogen to be a thermal short, thermometer heating due to carrier thermal conductance is then 0.037°C. The conductance is then simply:

$$\text{Conductance} = \frac{2 \times 10^{-3} \text{ W}}{3.7 \times 10^{-2} \text{ °C}} = 5.4 \times 10^{-2} \text{ W/°C}$$

This is interpreted as a requirement for a heat input of 0.5 mW for a temperature rise of less than 0.01°C which is a requirement on the heat-stationing of the thermometer leads.

Heat flow through sensor leads: The thermometers are connected to the Mueller bridge through four copper leads (per sensor). To estimate the required heat-stationing conductance, it is necessary to determine expected heat flow down these leads. From room-temperature environment to thermometer, the lead is approximately eight feet long. Cross-sectional diameter is 0.0125 inch, giving a cross-sectional area of 8.46 x 10^{-7} ft^2. The conductivity of copper is approximately 200 Btu/hr/°F/ft. The temperature gradient (worst-case) is approximately 200°C, or 360°F. The heat flow down a single lead is then:

$$\frac{dQ}{dt} = \frac{(2 \times 10^2)(8.46 \times 10^{-7})(3.6 \times 10^2) \text{ Btu/hr}}{4}$$

$$= 1.52 \times 10^{-2} \text{ Btu/hr}$$

In metric units,

$$\frac{dQ}{dt} = 2.2 \text{ mW/lead}$$

For four leads,

$$\frac{dQ}{dt} = 8.8 \text{ mW}$$

56

The conductance measurements yield a requirement that no more than 0.25 mW flow through the thermometer. The heat-stationing must be such that the ratio of the conductances be greater than 8.8/0.25 or 36:1. The lead will be heat-stationed on the source proper, with a secondary heat station on the guard heater.

Block conductivity. -- The setup for this measurement is shown in Figure 28. The experiment is designed to determine the gradient structure of the copper block with measured heat input. Three sets of measurement data were obtained - two sets with the thermometer and carrier in air and the third with the thermometer inserts filled with silicone oil. All measurements were made in the Honeywell Standards Laboratory at ambient temperature. In the first two sets the block was directly on the formica surface of the lab bench. In the third set the block was sitting on a cloth on the bench. The data is summarized in Figure 29 and is given in detail below.

Test No. 1, 22 November 1967

Power input, mW	Thermometer No. 631, °K	Thermometer No. 633, °K	ΔT, °K
0	296.4910	296.4931	.0021
47	296.5029	296.5079	.005
102.6	296.5365	296.5415	.005
192	296.5895	296.5988	.0093
414	296.6706	296.6868	.0162

Test No. 2, 27 November 1967

Power input, mW	Thermometer No. 631, °K	Thermometer No. 633, °K	ΔT, °K
0	296.84413	296.84446	.00033
48	296.83198	296.83460	.0026
105	296.8297	296.8326	.0029
200	296.8446	296.8499	.0053
445	296.9113	296.9235	.0122
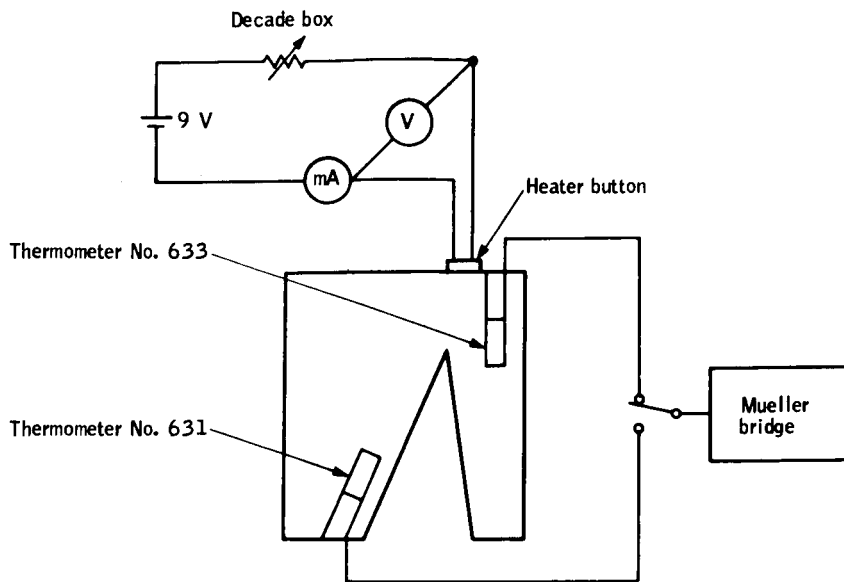
Figure 28. Block Conductivity Measurements
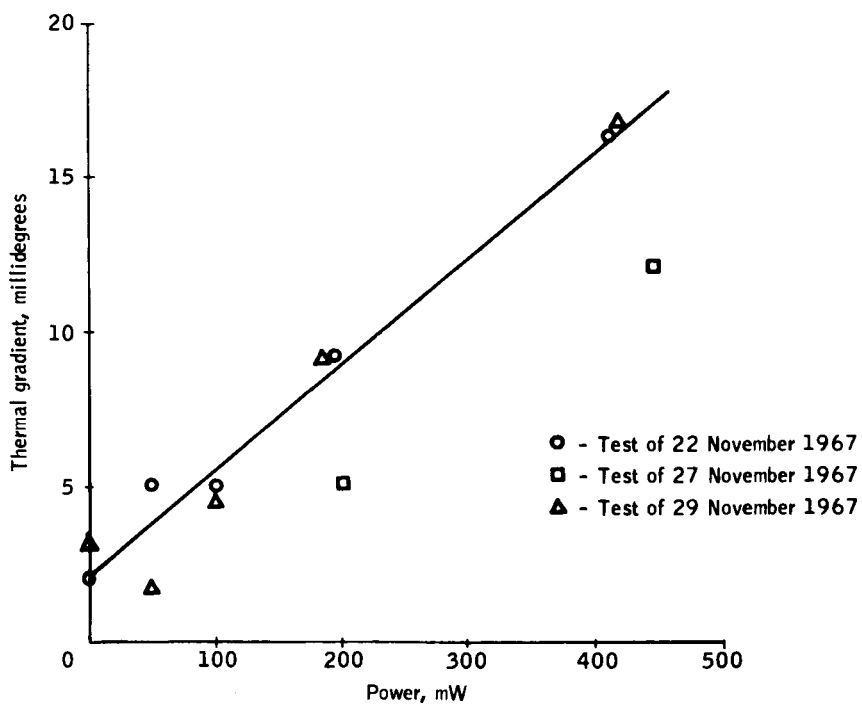
Figure 29. Temperature Gradient versus Power Input

Test No. 3, 29 November 1967

Power input, mW	Thermometer No. 631, °K	Thermometer No. 633, °K	ΔT, °K
0	296.4386	296.4417	.0031
46	296.4440	296.4457	.0017
102	296.4534	296.4580	.0046
184	296.4781	296.4864	.0083
420	296.5206	296.5375	.0169

The results of test no. 2 are anomalous. Note that temperature of the block was decreasing until 200 mW of heat were applied. The ambient temperature in the laboratory was exhibiting a downward drift at this time which apparently was showing up in the block temperature gradient structure. Test nos. 1 and 3 demonstrate excellent repeatability and are taken as indicative of the block gradient structure.

Radiometric Measurement

The aperture was mapped and the goniometric characteristics of the aperture scanned at three temperatures with the source in normal operating position. The source was rotated approximately 90° and the aperture map and goniometric characteristics measured at three temperatures. A block diagram of the experimental set-up is shown in Figure 30.
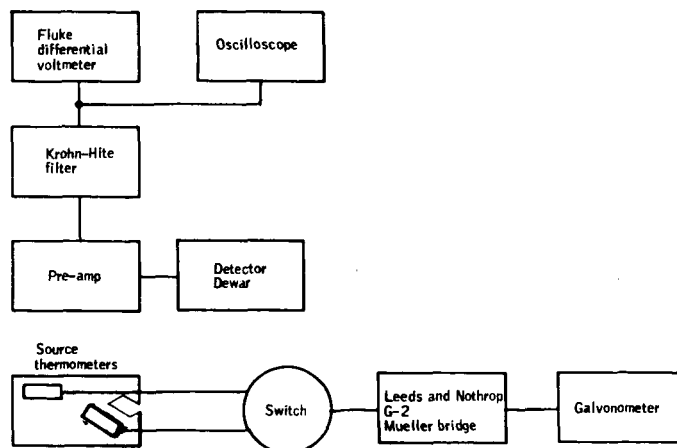
Figure 30. Experimental Set-up for Radiance Measurements

The detector output was amplified with a wide-band preamplifier and then narrowband filtered with a Krohn-Hite variable bandpass filter. Bandpass was set to obtain maximum signal/noise in the laboratory noise environment and was not measured. Bandpass was changed from the first set of measurements, making the responsivity vary. The voltages noted are only meaningful for any one set of data and cannot be correlated. The signal was then measured with a Fluke ac differential voltmeter. This voltmeter operates as a full-wave rectifier and low-pass filter. Simultaneously, temperatures on both platinum resistance thermometers were read with a Leeds and Northrop G-2 Mueller bridge and light-beam galvonometer.

Where required, data was reduced by converting temperature to radiance for each point. This operation was required because of the temperature drift encountered during this series of measurements. In addition, a significant thermal gradient was encountered during these tests (discussed separately below). In all cases, the temperature of the front thermometer was used in the normalization process.

The normalization was accomplished as follows. Assuming a linear relationship between voltage output and radiance inputs, the voltage obtained at scan center at temperature T_1 is

$$V(0, T_1) = k N(T_1)$$

and the voltage which would be obtained at scan center at temperature T_2 is

$$V(0, T_2) = k N(T_2)$$

Given the voltage measured at temperature T_2, where T_2 is known, the voltage that would have been measured had the system been at temperature T_1 is given by the identity:

$$V(0, T_1) = V(0, T_2) \frac{N(T_1)}{N(T_2)}$$

where $N(T_i)$ is the radiance and is a tabulated function.

For some angle θ other than scan center, the same relation will hold:

$$V(\theta, T_1) = V(\theta, T_2) \frac{N(T_1)}{N(T_2)}$$

It then can be shown that the radiance at θ, T_2, normalized to the radiance at scan center, is given by

$$N(\theta, T_1) = \frac{V(\theta, T_2)}{V(0, T_1)} \frac{N(T_1)}{N(T_2)} N(T_1)$$

That is, this radiance is the value that would be obtained at the position θ if the temperature when the measurement was taken was the same as the temperature when scan center was measured.

Within the test environment, stray noise (apparently rf pickup in the detector) limited resolution of the measurement to approximately 1 mV at the output. At room temperature, this corresponds to a measurement of one part in 500, and at the lowest temperature for which measurements were made (169°K) the measurement resolution was one part in 100.

The radiances measured range from 9 W/m^2-sr to 1 W/m^2-sr. The voltage resolution thus yields a radiance resolution between 0.02 and 0.01 W/m^2-sr.

Goniometric Characteristics

It can be shown that a Lambert radiator should yield constant flux in angle for an optical system in which the image of the radiator subtends a larger area than the detector. The condition is satisfied in the radiometer used here; the detector is 0.5 mm, source aperture 5 mm, and the system is operated at unity magnification. The measurement should then show constant output across the field.

Data was obtained with the source in normal operating position at temperatures 290.0, 241.9, and 169.5 °K. The source was then rotated 90° and data was obtained at temperatures of 289.8, 269, and 179.5 °K. Appendix A gives the raw data for these measurements. The voltages are plotted against angular position in Figures 31, 32 and 33.

In the first set of data (room temperature), Figure 31, a step function in voltage is evident. Examining the data taken on 3/20/68, this voltage step is evident at approximately the point of scan reversal. After this step, a reverse scan back to zero was made. This reverse scan is smooth. If the step is neglected, these data are smooth within the 1-mV precision of the reading. In the second set of data (240 to 270°K) the effects of temperature drift are evident and a correction must be applied to make meaningful statements regarding this data. The third set of data (170°K) does not exhibit temperature or voltage anomalies and shows an angular dependence which is as expected. The data of Figure 32 has been temperature-corrected as discussed above and is given in Figure 34. An anomaly is still present in the initial downward scan in both data sets. The data taken on 3/18/68 does yield a scan which is flat through the full angular range.

An attempt was made to correlate the anomalies in two sets of data with temperature gradients in the source (see Thermal Gradient section). There is no correlation evident.
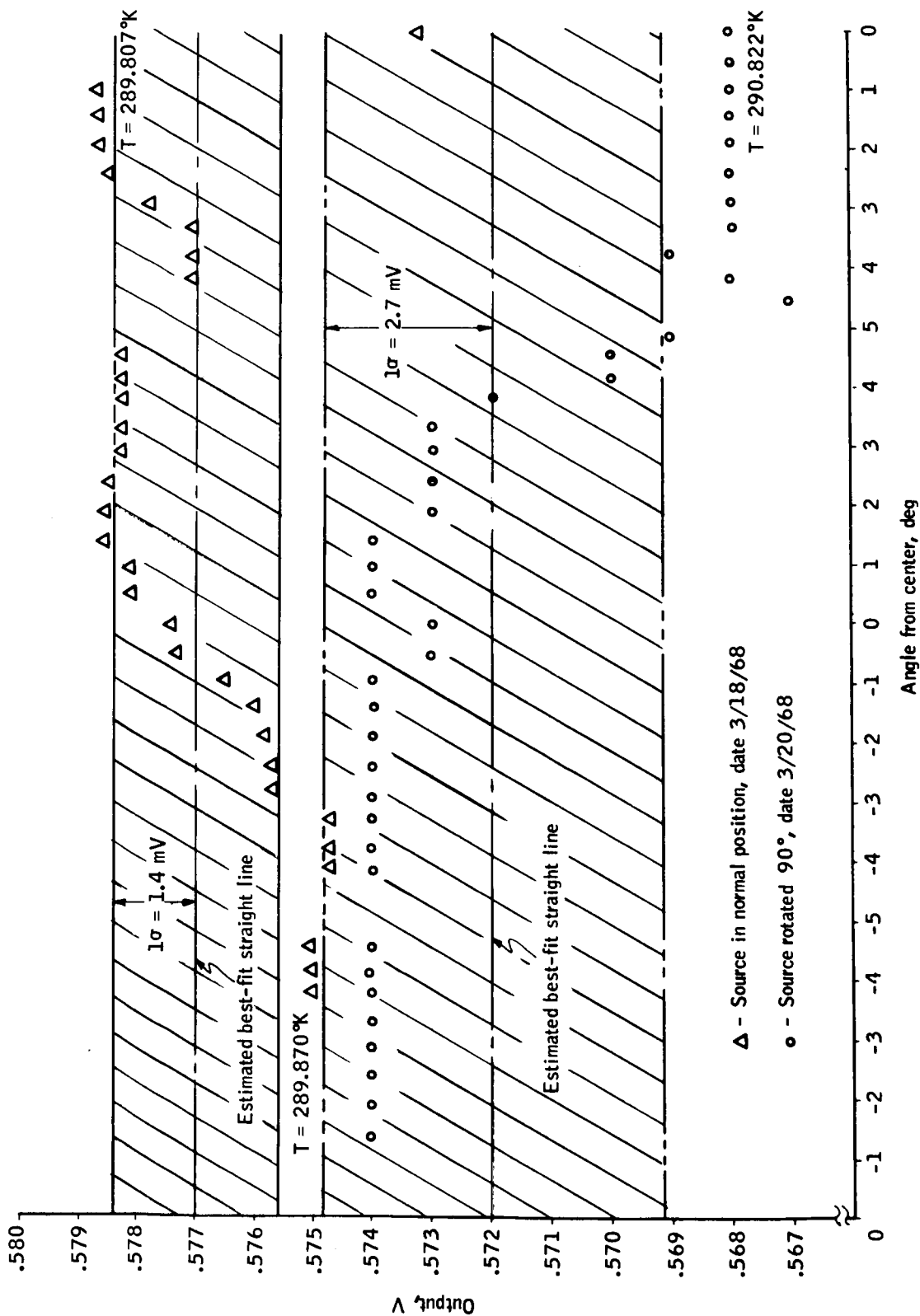
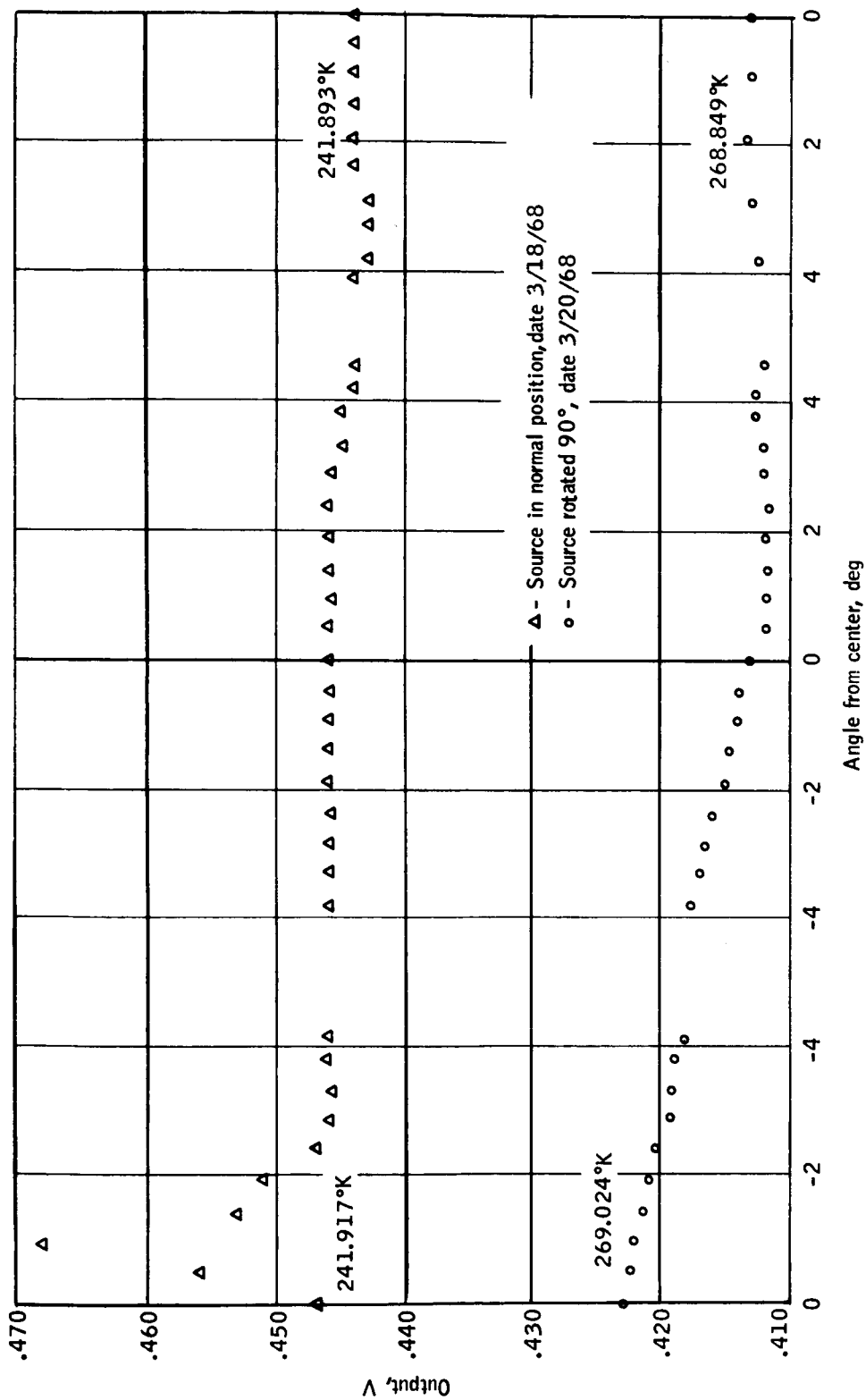61

Figure 31. Output Voltage as a Function of Angle

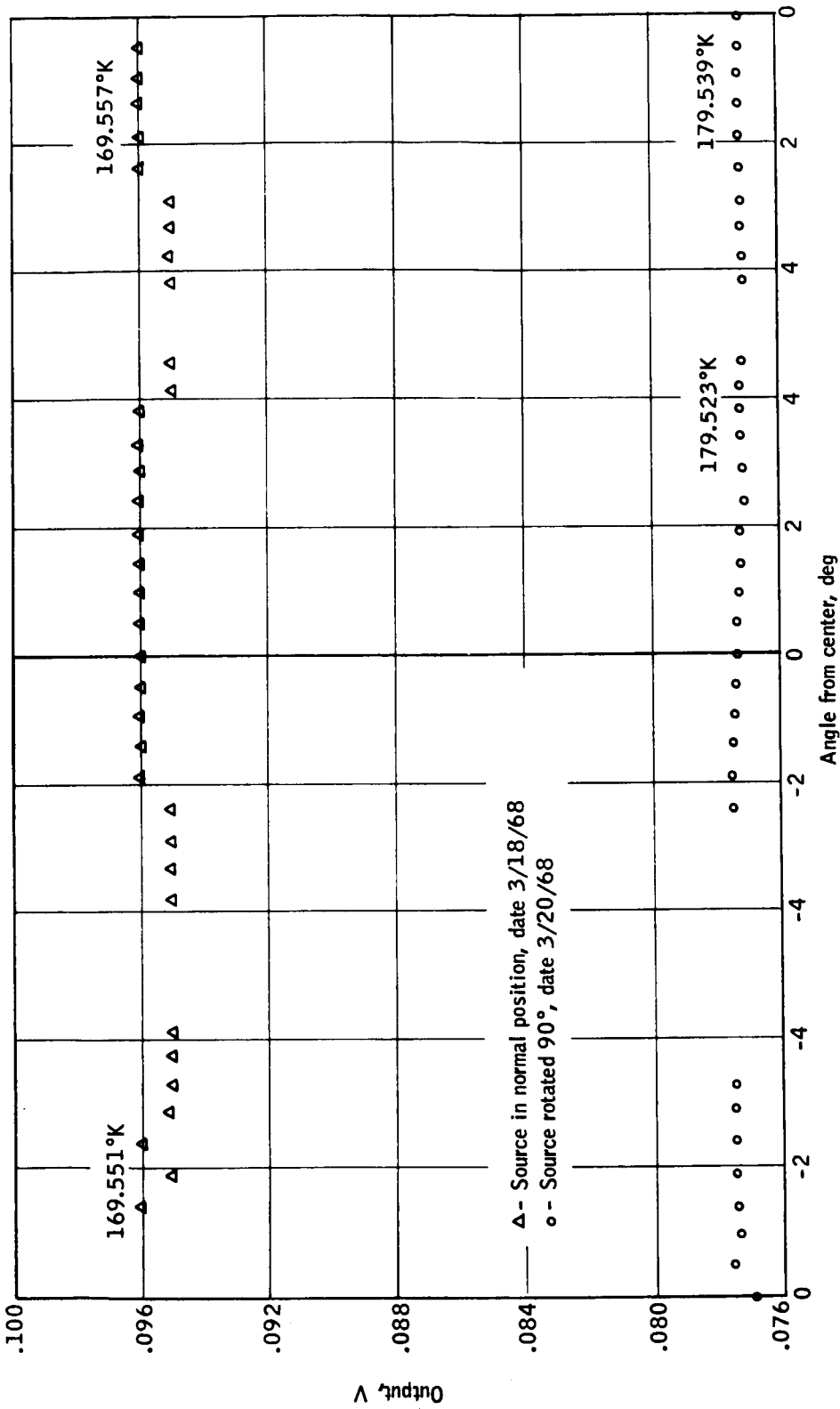Figure 32. Output Voltage as a Function of Angle

Figure 33. Output Voltage as a Function of Angle
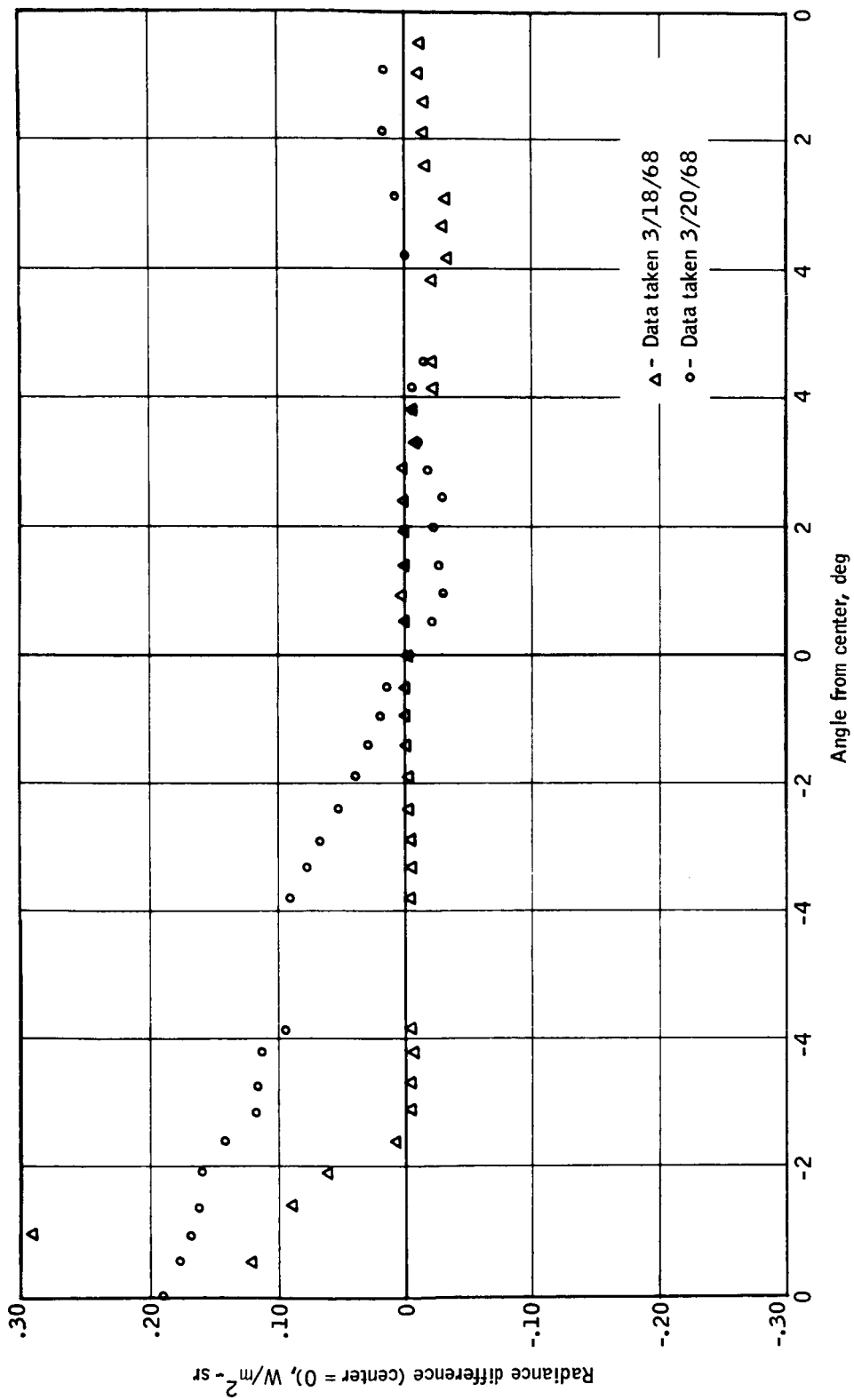
Figure 34. Corrected Radiance Difference as a Function of Angle

The steps in voltage seen in two sets of data are apparently correlated with the settling time of the electrical grounding system when a tool is introduced to make the angular changes. There also appears to be some correlation with dc shifts and the end of travel of the source. End of travel upward is determined by mechanical interference and this effect may be explainable in terms of forming new ground paths when the source structure makes mechanical contact with the liquid-nitrogen shrouds. Fortunately, for every anomaly in the data there is a second set of equivalent data which displays constant behavior at the same angles and temperature. Then, although interpretation is required, there appears to be sufficient evidence in the above data sets to draw the conclusion that the system exhibits the desired flat characteristic over a 10° range of angles throughout the temperature range from 290 to 170°K, within approximately 0.02 W/m^2-sr. Further testing in a cleaner electrical environment is clearly required to make the above statement with statistical confidence. The rms deviation of the data about a best-fit (hand-drawn) straight line has been computed with the above anomalous conditions included for the high-temperature set of data and is shown in this figure. The rms deviation for both sets of data taken together is approximately 2 mV or, assuming a linear voltage-radiance relationship, approximately 0.04 W/m^2-sr. For the source in its normal position, the rms deviation is approximately 3 mV, or 0.06 W/m^2-sr, and for the source rotated 90°, 1.4 mV or 0.028 W/m^2-sr.

Aperture Scan

The aperture was scanned in 0.025-inch (0.64-mm) steps at 241.9 and 169.5°K. Appendix A gives the raw data for these measurements. The voltages are plotted against scan position in Figures 35, 36, and 37. Also shown on these figures are the mechanical sizes of the aperture and detector. There is essentially perfect correlation with expected results. The aperture demonstrates no gradients throughout the range.

THERMAL GRADIENT

An unexplained thermal gradient varying between approximately 15 and 20 millidegrees was present in the source during the measurements described above. The rear thermometer was consistently reading lower than the front. The gradient is a function of source temperature, being larger at warmer source temperatures. Figures 38 and 39 show representative data.

The system was disassembled and inspected. The heater, control thermometers, and precision thermometer wiring was redone to isolate these wires from possible contact with liquid-nitrogen lines and from each other. The gradient was still present during temperature stabilization of the source after this rework.

The system was completely disassembled and the thermometers calibrated

66
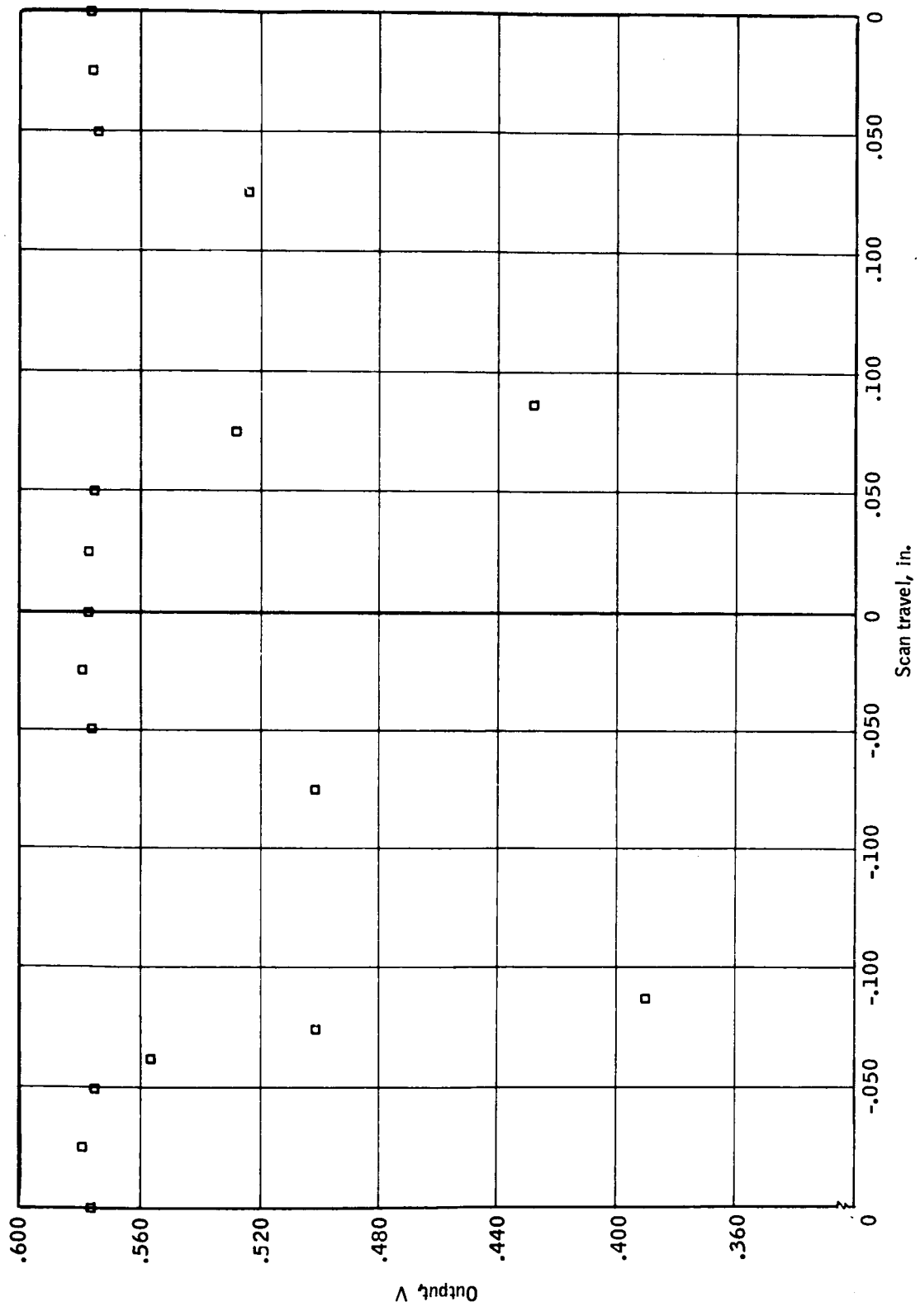
Figure 35. Output Voltage as a Function of Position in the Aperture (Temperature 290°K)
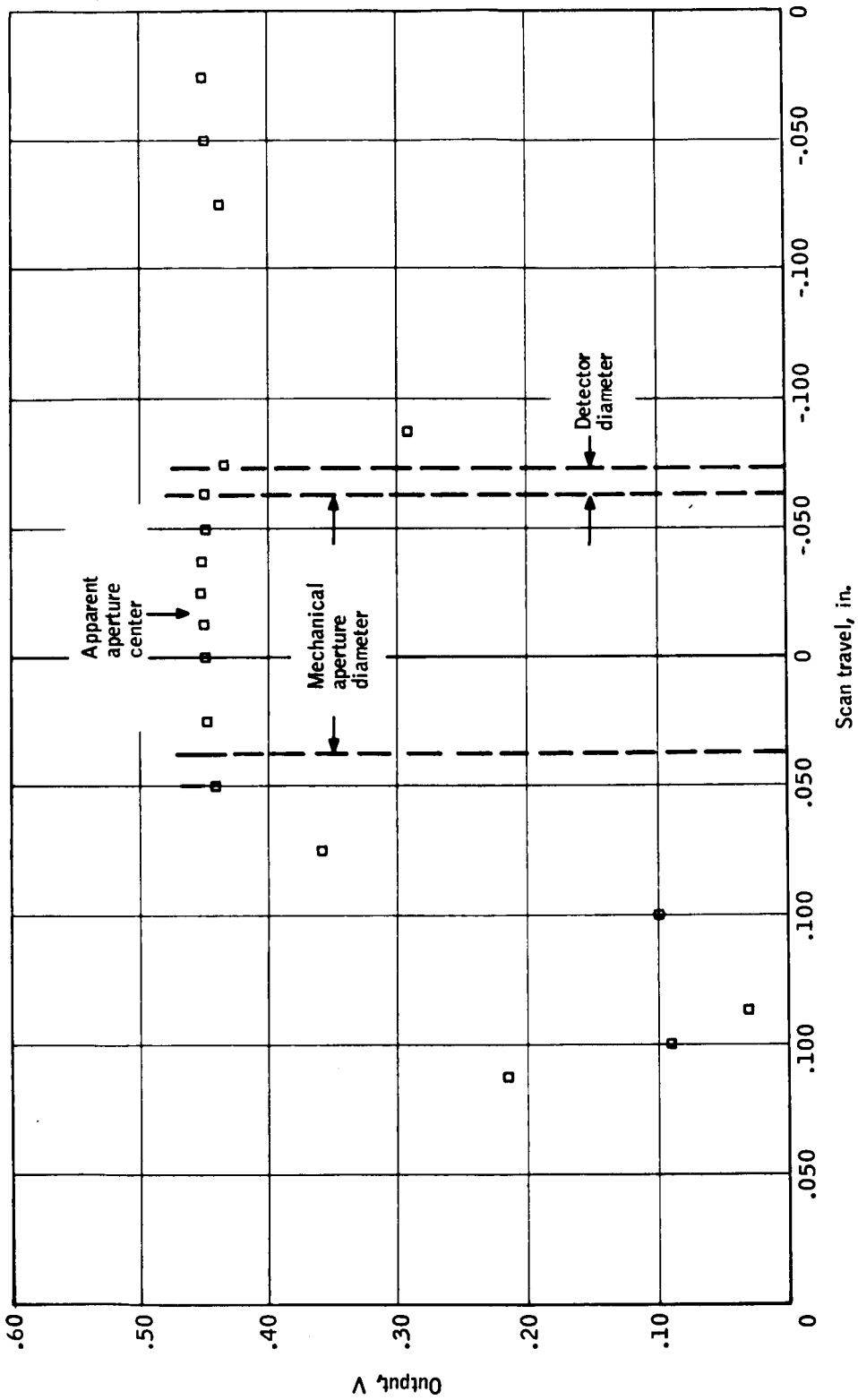
Figure 36. Output Voltage as a Function of Position in the Aperture (Temperature 241.9°K)
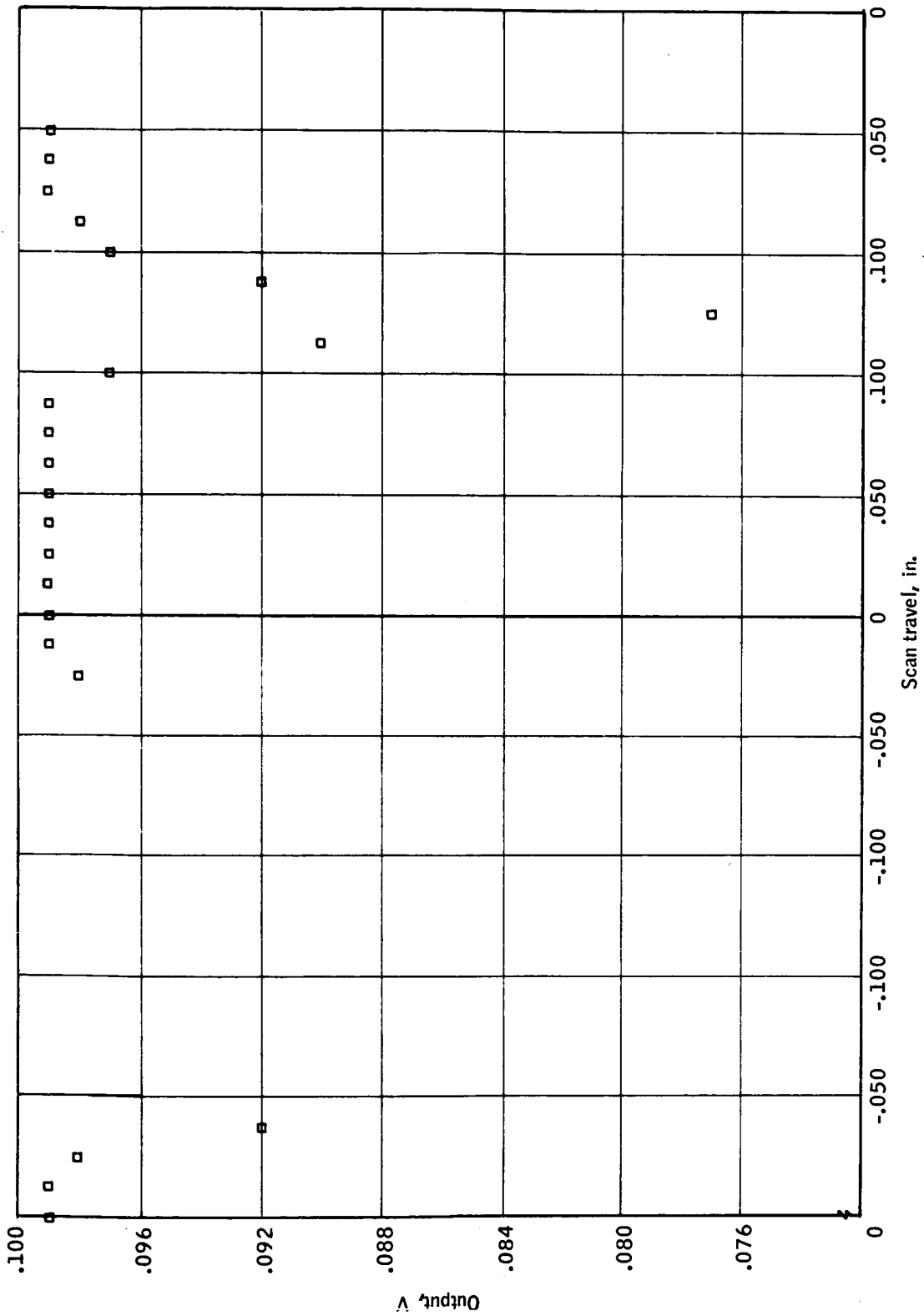
Figure 37. Output Voltage as a Function of Position in the Aperture (Temperature 169°K)
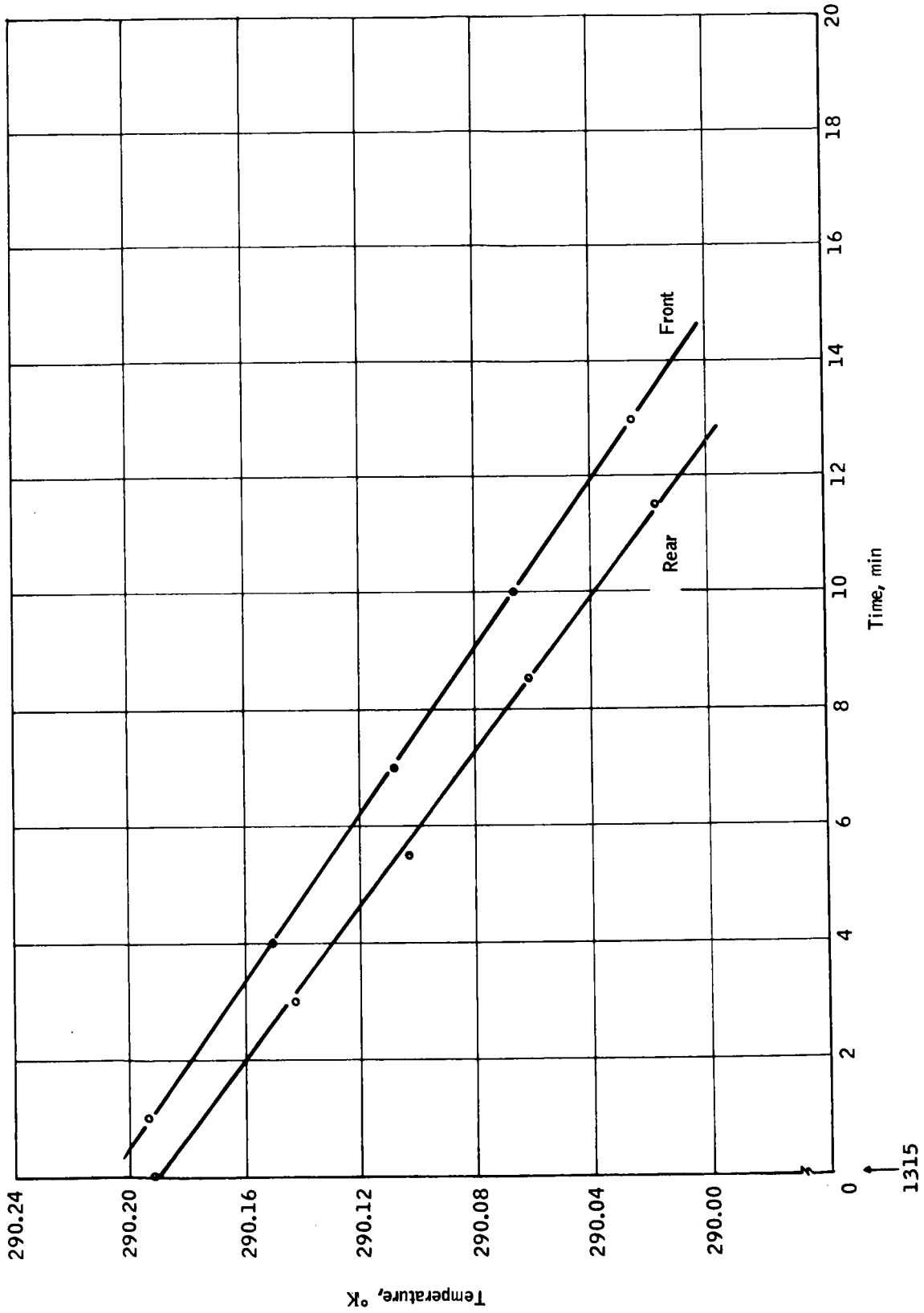
Figure 38. Thermal Gradient at Room Temperature
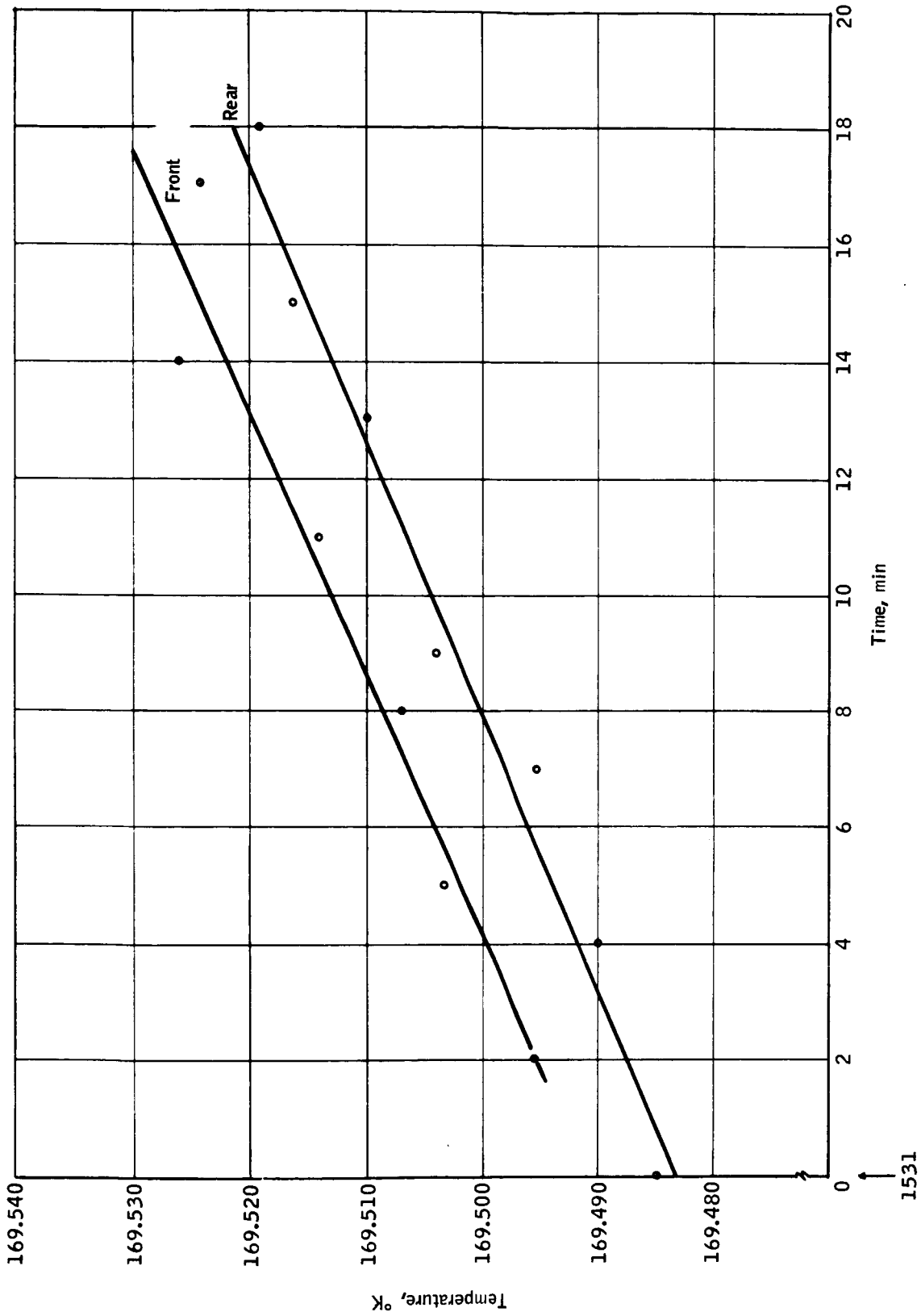
Figure 39. Thermal Gradient at Low Temperature

71

against a certified standard in an ice bath. Both thermometers had shifted calibration, and the differential shift was approximately six millidegrees. The absolute shift was approximately 15 millidegrees. This is not sufficient to explain the problem. From the manner in which the gradient exists, it appears that a thermal short from the rear of the block to liquid-nitrogen lines is the cause. It is recommended that the liquid-nitrogen lines be wrapped with fiberglass to isolate this source of error.

The absolute shift of the thermometers makes the thermometry state of the art suspect in this application. It should be noted that, because of delivery difficulties, the thermometers used were nonstandard in that the operating range was limited at the high temperature to 350°K. As a consequence, these thermometers could not be annealed. The manufacturer states that an unannealed thermometer would be subject to change due to mechanical stress. It is recommended that these thermometers be subjected to drift testing and be recalibrated periodically.

APPENDIX A

RADIOMETRIC TEST DATA FOR APERTURE AND
ANGULAR SCANS OF THE CAVITY

TABLE A1. - ANGULAR SCAN

Time, 3/20/68	Front thermometer temperature, °K	Rear thermometer temperature, °K	Output voltage, V	Angle, deg
1552			.0770	0
1552			.0776	-0.50
1553			.0774	-0.95
1553			.0774	-1.4
1553			.0775	-1.9
1554			.0775	-2.4
1554			.0775	-2.9
1554			.0775	-3.3
1554			.0775	-2.4
1554			.0775	-1.9
1555			.0775	-1.4
1555		179.500	.0774	-0.95
1555			.0774	-0.50
1556			.0773	0
1556			.0773	0.50
1556			.0773	0.95
1556			.0772	1.4
1556			.0772	1.9
1557			.0771	2.4
1557	179.523		.0771	2.9
1557			.0772	3.3
1557			.0772	3.8
1558			.0772	4.15
1558			.0771	4.55
1558			.0771	4.15
1558			.0771	3.8
1559			.0772	3.3
1559		179.517	.0772	2.9
1559			.0772	2.4
1600			.0772	1.9
1600	179.539		.0772	1.4
1600			.0772	0.95
1600			.0772	0.50
1600			.0772	0

TABLE A2. - ANGULAR SCAN

Time, 3/20/68	Front thermometer temperature, °K	Rear thermometer temperature, °K	Output voltage, V	Angle, deg
1409			.4230	0
1409		268.994	.4223	-0.50
1409			.4218	-0.95
1410			.4214	-1.4
1410	269.003		.4207	-1.9
1410			.4203	-2.4
1411			.4191	-2.9
1411			.4190	-3.3
1412			.4188	-3.8
1412			.4180	-4.15
1412			.4176	-3.8
1413			.4170	-3.3
1413			.4165	-2.9
1413			.4159	-2.4
1414			.4150	-1.9
1414			.4146	-1.4
1414			.4141	-0.95
1415			.4138	-0.50
1415			.4131	0
1416			.4120	0.50
1416			.4117	0.95
1416			.4118	1.4
1417			.4119	1.9
1417		268.875	.4116	2.4
1417			.4120	2.9
1418			.4123	3.3
1419			.4125	3.8
1419	268.886		.4123	4.15
1419			.4119	4.55
1420			.4124	3.8
1420		268.836	.4128	2.9
1420			.4131	1.9
1421			.4130	0.95
1421	268.849		.4131	0

TABLE A3. - ANGULAR SCAN

Time, 3/20/68	Front thermometer temperature, °K	Rear thermometer temperature, °K	Output voltage, V	Angle, deg
1340			.576	-0.50
1340			.576	-0.95
1340			.574	-1.4
1340			.574	-1.9
1340			.574	-2.4
1340			.574	-2.9
1340			.574	-3.3
1341			.574	-3.8
1341			.574	-4.15
1341		289.827	.574	-4.55
1341			.574	-4.15
1341			.574	-3.8
1341			.574	-3.3
1342			.574	-2.9
1342			.574	-2.4
1342			.574	-1.9
1342	289.843		.574	-1.4
1342			.574	-0.95
1342			.573	-0.50
1343			.573	0
1343			.574	0.50
1343			.574	0.95
1343			.574	1.4
1343			.573	1.9
1343		289.791	.573	2.4
1343			.573	2.9
1343			.573	3.3
1343			.572	3.8
1343			.570	4.15
1343			.570	4.55
1343			.569	4.85
1344			.567	4.55
1344			.568	4.15
1344			.569	3.8
1344			.568	3.3
1344			.568	2.9
1344	289.807		.568	2.4
1344			.568	1.9
1344			.568	1.4
1344			.568	0.95
1344			.568	0.50
1344			.568	0

TABLE A4. - APERTURE SCAN

Time, 3/20/68	Front thermometer temperature, °K	Rear thermometer temperature, °K	Output voltage, V	Position, inches
1334			.577	0
1334			.579	-.025
1335			.576	-.050
1335			.556	-.0625
1335			.501	-.075
1335			.390	-.0875
1336			.501	-.075
1336			.576	-.050
1336			.579	-.025
1337			.578	0
1337	289.917		.577	.025
1337			.576	.050
1337			.528	.075
1338		289.874	.428	.0875
1338			.524	.075
1339			.575	.050
1339	289.886		.576	.025
1339			.577	0

TABLE A5. - APERTURE SCAN

Time, 3/18/68	Front thermometer temperature, °K	Rear thermometer temperature, °K	Output voltage, V	Position, inches
1659		241.924	.449	0
1700			.449	.0125
1700			.448	.025
1700			.448	.0375
1701			.441	.050
1701			.414	.0625
1702	241.945		.352	.075
1702			.214	.0875
1703		241.908	.089	.100
1704			.029	.1125
1704			.098	.100
1705			.356	.075
1705	241.931		.442	.050
1706			.447	.025
1706			.449	0
1707			.449	-.0125
1707			.451	-.025
1707		241.898	.450	-.0375
1707			.449	-.050
1707			.448	-.0625
1707			.433	-.075
1708			.291	-.0875
1709			.437	-.075
1709			.449	-.050
1709	241.919		.449	-.025
1709			.448	0

TABLE A6. - APERTURE SCAN

Time, 3/18/68	Front thermometer temperature, °K	Rear thermometer temperature, °K	Output voltage, V	Position, inches
1534			.099	.050
1534			.099	.0375
1534			.099	.029
1535			.099	.0125
1535			.099	0
1535		169.509	.099	-.0125
1535			.098	-.025
1535			.092	-.0375
1536	169.528		.098	-.025
1537			.099	-.0125
1537	169.529		.099	0
1537			.099	.0125
1537			.099	.025
1538			.099	.0375
1538			.099	.050
1538		169.514	.099	.0625
1538			.099	.075
1538			.099	.0875
1538			.097	.100
1539			.090	.1125
1539	169.532		.077	.125
1539			.050	.1375
1540			.077	.125
1540		169.523	.092	.1125
1540			.097	.100
1541			.098	.0875
1541			.099	.075
1541			.099	.0625
1542	169.539		.099	.050

TABLE A7. - ANGULAR SCAN

Time, 3/18/68	Front thermometer temperature, °K	Rear thermometer temperature, °K	Output voltage, V	Angle, deg
1710		241.890	.447	0
1710			.456	-0.50
1711			.468	-0.95
1712			.453	-1.4
1712	241.912		.451	-1.9
1713			.447	-2.4
1713			.446	-2.9
1713			.446	-3.3
1713			.446	-3.8
1713			.446	-4.15
1713			.446	-3.8
1713			.446	-3.3
1714			.446	-2.9
1714			.446	-2.4
1714			.446	-1.9
1714			.446	-1.4
1714			.446	-0.95
1714		241.883	.446	-0.50
1714			.446	0
1714			.446	0.50
1715			.446	0.95
1715			.446	1.4
1715			.446	1.9
1715	241.904		.446	2.4
1715			.446	2.9
1715			.445	3.3
1716			.445	3.8
1716			.444	4.15
1716			.444	4.55
1716			.444	4.15
1716			.444	3.8
1717			.443	3.3
1717			.443	2.9
1717			.443	2.4
1717		241.874	.444	1.9
1717			.444	1.4
1717			.444	0.95
1718	241.893		.444	0.50

TABLE A8. - ANGULAR SCAN

Time, 3/18/68	Front thermometer temperature, °K	Rear thermometer temperature, °K	Output voltage, V	Angle, deg
1544			.096	0
1544		169.529	.096	-0.50
1544			.096	-0.95
1545			.096	-1.4
1545			.095	-1.9
1545	169.551		.096	-2.4
1545			.095	-2.9
1545			.095	-3.3
1545			.095	-3.8
1546			.095	-4.15
1546			.095	-3.8
1546			.095	-3.3
1546		169.535	.095	-2.9
1546			.095	-2.4
1546			.096	-1.9
1546			.096	-1.4
1547			.096	-0.95
1547			.096	-0.50
1547			.096	0
1547			.096	0.50
1547			.096	0.95
1547			.096	1.4
1548			.096	1.9
1548			.096	2.4
1548	169.549		.096	2.9
1548			.096	3.3
1548			.096	3.8
1549			.095	4.15
1549		169.538	.095	4.55
1549			.095	4.15
1550			.095	3.8
1550			.095	3.3
1550			.095	2.9
1550			.096	2.4
1550			.096	1.9
1550			.096	1.4
1551			.096	0.95
1551			.096	0.50

82

TABLE A9. - ANGULAR SCAN

Time, 3/18/68	Front thermometer temperature, °K	Rear thermometer temperature, °K	Output voltage, V	Angle, deg
1337			.5779	0
1337			.5779	-0.50
1337		290.898	.5770	-0.95
1337			.5765	-1.4
1338			.5761	-1.9
1338			.5756	-2.4
1338			.5751	-2.9
1339			.5750	-3.3
1339			.5750	-3.8
1339			.5750	-4.15
1339	290.909		.5750	-4.55
1340			.5747	-4.15
1340			.5747	-3.8
1340			.5747	-3.3
1340			.5757	-2.9
1341			.5757	-2.4
1341			.5758	-1.9
1341		290.862	.576	1.4
1341			.5765	-0.95
1342			.5773	-0.50
1342			.5774	0
1343			.5781	0.50
1343	290.880		.5781	0.95
1343			.57857	1.4
1344			.57855	1.9
1344		290.862	.57850	2.4
1344			.57825	2.9
1344			.57825	3.3
1345			.57825	3.8
1345			.57825	4.15
1345			.57825	4.55
1345			.57705	4.15
1346			.57705	3.8
1346	290.845		.57705	3.3
1346			.57705	2.9
1347			.57778	2.4
1347		290.785	.57850	1.9
1347			.57867	1.4
1347			.57870	0.95
1348			.57870	0.50
1348	290.822		.57840	0

APPENDIX B
DETECTOR CHARACTERISTICS

(From Data Supplied by Santa Barbara Research Center,
75 Cormar Drive, Goleta, California)

APPENDIX B
DETECTOR CHARACTERISTICS

DETECTOR SERIAL NUMBER ____0187____   DATE ____12 October 1967____

DETECTOR CONSTRUCTION

Type	Ge:Cu	Total field of view	10°
Vacuum flask style	9145-1SS2	Window material	KRS-5
Filters	Special	Area, cm^2	1.96×10^{-3}
Sensitive area configuration	0.5 mm diam.		

DETECTOR ELECTRICAL PARAMETERS		CONDITIONS OF MEASUREMENT	
Noise equivalent power, W	3.28×10^{-12}	Blackbody temperature, °K	500
Detectivity, cm - $Hz^{1/2}$/W	1.35×10^{10}	Chopping frequency, Hz	1800
Detectivity, λ_m, cm - $Hz^{1/2}$/W	--	Bandwidth, Hz	1
Responsivity, V/W	6.97×10^4	Detector temperature, °K	4.3
Responsivity, λ_m, V/W	--	Ambient temperature, °K	295
Resistance, E/I, megohms	1.87	Load resistance, megohms	1
Time constant, μ sec	--	Detector current, μA	8.7
Signal, μV	4000	Applied voltage, volts (detector + load)	25
Noise, μV	2.29		
Signal-to-noise ratio	1.75×10^3	Blackbody flux density, μW/cm^2	2.93

NOTES:

1. Window is antireflection coated for peak transmission at _____ microns.

2. Unless otherwise indicated, detectivity is maximized for the blackbody temperature and chopping frequency shown.

3. Applied voltage indicated is across both the detector and load resistance in series.

4. For all correspondence relative to this detector, please refer to SBRC W/A 5029.

5. Customer P.O. No. PDY-575507.

6. Customer: Honeywell Inc.

Deposition no. __0187__

Cell no. _____

Substrate material __Ge:Cu__

Cell size __0.5 mm diam.__

Blackbody temperature __500°K__

Flux density __2.93 μW/cm²__

Date	R_{in}, MΩ	R_{load}, MΩ	Cell I, μA	E, V	Chop freq, Hz	Band pass, Hz	Noise, μV	Sig, μV	S/N	D^*	Bias Polarity
10/10/67	3.17	1	1.2	5	1800	6	1.3	660	508		–
	3.17	1	1.2	5	1800	6	1.4	660	472		+
	2.57	1	2.8	10	1800	6	2.4	1350	562		–
	2.47	1	3.6	12.5	1800	6	3.2	1775	554		–
	2.41	1	4.4	15	1800	6	3.6	2175	603		–
	2.15	1	5.4	17.5	1800	6	4.4	2600	591	1.34×10^{10}	–
	2.12	1	6.4	20	1800	6	4.5	3100	688		–
	1.87	1	8.7	25	1800	6	5.6	4000	713		–
	1.68	1	11.2	30	1800	6	7.0	4600	658		–
	1.41	1	14.5	35	1800	6	8.6	5000	582		–
	1.28	1	17.5	40	1800	6	10.0	4800	480		–

Ge:Cu Detector S/N 0189 14-16μ Filter

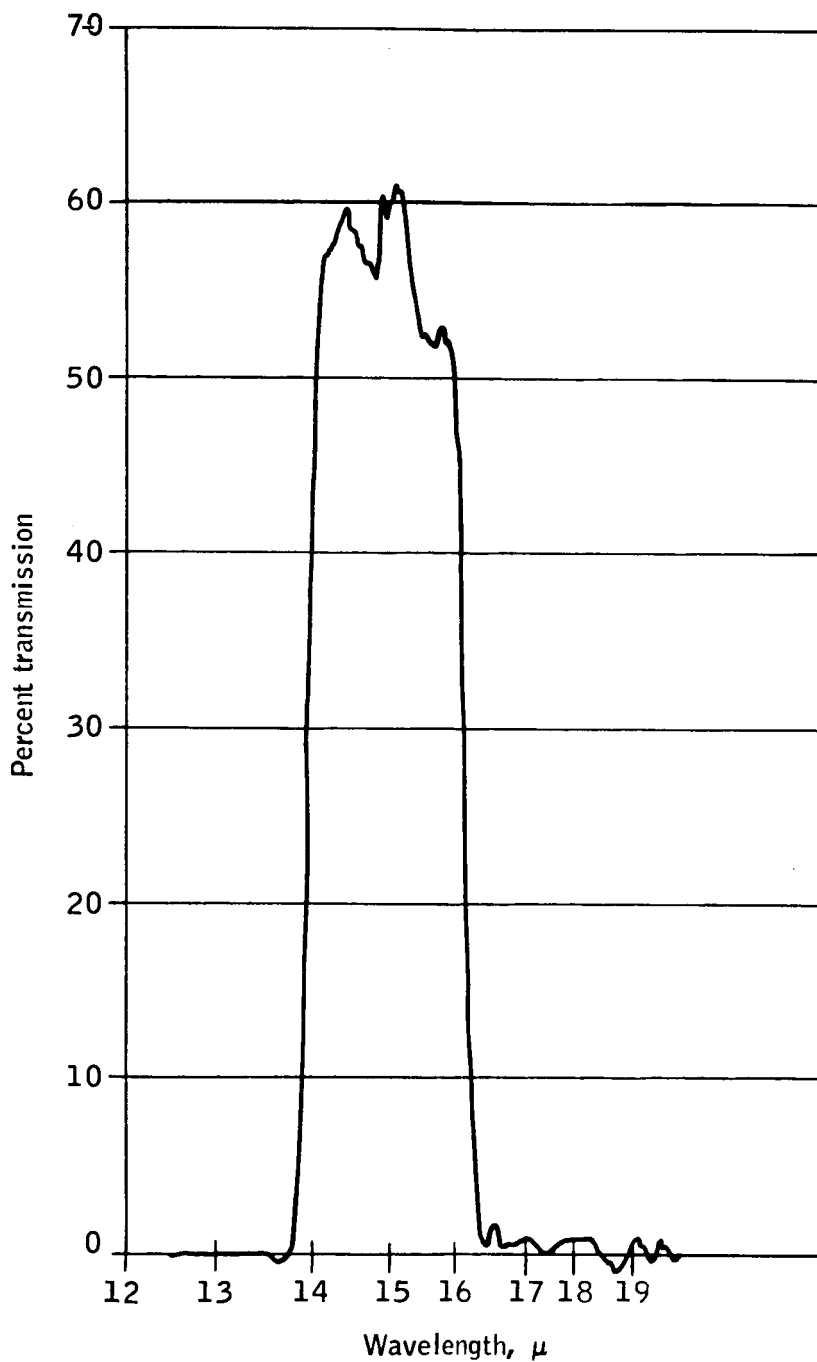| Wavelength	Relative response	Normalized response, %
13.5	0	0.0
0.6	1	1.4
0.7	3	4.2
0.8	5	7.0
0.9	13	18.0
14.0	17	24.0
0.1	28	39.0
0.2	36	50.0
0.3	44	61.0
0.4	48	67.0
0.5	50	69.0
0.6	50	69.0
0.7	50	69.0
0.8	52	72.0
0.9	56	78.0
15.0	52	72.0
0.1	54	75.0
0.2	57	79.0
0.3	62	86.0
0.4	54	75.0
0.5	51	71.0
0.6	53	74.0
0.7	72	100.0
0.8	60	83.0
0.9	57	79.0
16.0	44	61.0
0.1	27	37.0
0.2	13	18.0
0.3	10	14.0
0.4	4	5.5
0.5	2	2.8
0.6	1	1.4
0.7	0	

Figure B1.   Spectral Response of 14 to 16μ Filter

REFERENCES

1. McKee, Thomas B.; Whitman, Ruth I.; and Davis, Richard E.: Preliminary Infrared Horizon Profiles from Project Scanner. NASA TM X-1483, December 1967.

2. Bates, Jerry C.; Hanson, David S.; House, Fred B.; Carpenter, Robert O'B.; Gille, John C.: The Synthesis of 15μ Infrared Horizon Radiance Profiles from Meteorological Data Inputs. NASA CR-724, October 1966.

3. Carson, John C.; Titus, Joseph S.; Mooers, Alden J.; Peterson, Ralph W.; West, Charles N.; and Jansson, Richard M.: Feasibility Design of an Instrument System for Measurement of Horizon Radiance in the CO_2 Absorption Band. NASA CR-66 429, May 1967.

4. Stinson, H. F.: The International Temperature Scale of 1948. National Bureau of Standards Handbook 77, Volume II, 1 February 1961.

5. Wildback, W. A.; Powell, R. C.; and Mason, H. L., ed.: Accuracy in Measurements and Calibrations, NBS Technical Note 262, 15 June 1965.

6. Eckert, Ernst R.: Introduction to the Transfer of Heat and Mass. McGraw-Hill, 1950.